Heavy-quark free energy, Debye mass, and spatial string tension at finite temperature in two flavor lattice QCD with Wilson quark action

Y. Maezawa,[1] N. Ukita,[2] S. Aoki,[3,4] S. Ejiri,[5] T. Hatsuda,[1] N. Ishii,[2] and K. Kanaya[3]

(WHOT-QCD Collaboration)

[1]*Department of Physics, The University of Tokyo, Tokyo 113-0033, Japan*
[2]*Center for Computational Sciences, University of Tsukuba, Tsukuba, Ibaraki 305-8577, Japan*
[3]*Graduate School of Pure and Applied Sciences, University of Tsukuba, Tsukuba, Ibaraki 305-8571, Japan*
[4]*RIKEN BNL Research Center, Brookhaven National Laboratory, Upton, New York 11973, USA*
[5]*Physics Department, Brookhaven National Laboratory, Upton, New York 11973, USA*
(Received 13 February 2007; published 6 April 2007)

We study Polyakov loop correlations and spatial Wilson loop at finite temperature in two-flavor QCD simulations with the RG-improved gluon action and the clover-improved Wilson quark action on a $16^3 \times 4$ lattice. From the line of constant physics at $m_{\rm PS}/m_{\rm V} = 0.65$ and 0.80, we extract the heavy-quark free energies, the effective running coupling $g_{\rm eff}(T)$ and the Debye screening mass $m_D(T)$ for various color channels of heavy quark-quark and quark-antiquark pairs above the critical temperature. The free energies are well approximated by the screened Coulomb form with the appropriate Casimir factors at high temperature. The magnitude and the temperature dependence of the Debye mass are compared to those of the next-to-leading-order thermal perturbation theory and to a phenomenological formula in terms of $g_{\rm eff}(T)$. We make a comparison between our results with the Wilson quark action and the previous results with the staggered quark action. The spatial string tension is also studied in the high temperature phase and is compared to the next-to-next-leading-order prediction in an effective theory with dimensional reduction.

DOI: 10.1103/PhysRevD.75.074501 PACS numbers: 11.15.Ha, 12.38.Gc, 12.38.Mh

I. INTRODUCTION

Recent relativistic heavy-ion experiments have revealed various remarkable properties of QCD at finite temperatures and densities, suggesting the realization of the QCD phase transition from the hadronic matter to the quark-gluon plasma (QGP) [1]. In order to extract unambiguous signals for the transition from the heavy-ion experiments, it is indispensable to make a quantitative calculation of the thermal properties of QGP from the first principles. Currently, the lattice QCD simulation is the only systematic method to do so. By now, most of the lattice QCD studies at finite temperature and chemical potential have been performed using staggered quark actions with the fourth-root trick of the quark determinant, which require less computational costs than others. However the lattice artifacts of the staggered quark actions are not fully understood. Therefore, it is important to compare the results from other lattice quarks such as Wilson quark actions to control and estimate the lattice discretization errors.

Such a study at finite temperature ($T \neq 0$) and zero chemical potential ($\mu_q = 0$) has been initiated several years ago using the Iwasaki (RG) improved gauge action and the $N_f = 2$ clover-improved Wilson quark action by the CP-PACS Collaboration [2,3]. The phase structure, the transition temperature and the equation of state have been investigated in detail, and also the crossover scaling around the chiral phase transition has been tested. In contrast to the case of staggered quark actions, the subtracted chiral condensate in the standard Wilson quark action [4] and in the clover-improved Wilson quark action [2] shows the scaling behavior with the critical exponents and scaling function of the three-dimensional O(4) spin model. This suggests that the lattice QCD with Wilson-type quarks is in the same universality class as the O(4) spin model, as expected from the effective sigma model analysis [5,6]. Moreover, extensive calculations of various physical quantities at $T = 0$ such as the light hadron masses have been carried out using the same action [7,8].

Since a lot of experimental results are obtained by the heavy-ion collisions and numbers of technical progresses in treating system at finite baryon density on the lattice have been made after the studies by the CP-PACS Collaboration, it is worth while to revisit the QCD thermodynamics with Wilson quark actions. In particular, it is essential to perform simulations along the lines of constant physics (LCP) to clearly extract the temperature- and density-dependences. As a first step in this direction, we carry out simulations of $N_f = 2$ QCD on an $N_s^3 \times N_t = 16^3 \times 4$ lattice at $m_{\rm PS}/m_{\rm V} = 0.65$ and 0.80 in the range $T/T_{\rm pc} \sim 0.76$–4.0, where $m_{\rm PS}$ ($m_{\rm V}$) is the pseudoscalar (vector) meson mass and $T_{\rm pc}$ is the pseudocritical point along the LCP. Among various topics which can be studied using the above configurations, we will focus on two subjects in this paper: the free energy between heavy quarks and the spatial string tension. They are the fundamental

quantities to characterize the perturbative and nonperturbative properties of the hot QCD medium.

The heavy-quark free energy was recently studied by lattice simulations in the quenched approximation [9–11], and in full QCD with the staggered quark action [12,13] and with the Wilson quark action [14]. An analytic study based on the thermal perturbation theory was also reported [15]. It was pointed out that the interaction between heavy quarks is intimately related to the fate of charmoniums and bottomoniums in QGP created in relativistic heavy-ion collisions [16]. In this paper, we make a systematic study of the free energy between a quark (Q) and an antiquark ($\bar{Q}$) in the color-singlet and octet channels, and between Q and Q in the color antitriplet and sextet channels. We adopt the Coulomb gauge fixing for the gauge-non-singlet free energies. By fitting the numerical results with a screened Coulomb form, we extract an effective running coupling and the Debye screening mass in each channel as functions of temperature. We also study the ''force'' between heavy quarks defined through the derivative of the free energy with respect to the interquark distance. We show that (i) the free energies in the different channels at high temperature ($T \gtrsim 2T_{\rm pc}$) can be well described by channel-dependent Casimir factors together with the channel-independent running coupling $g_{\rm eff}(T)$ and Debye mass $m_D(T)$, (ii) the next-to-leading-order result of the Debye mass in thermal perturbation theory agrees better with the lattice $m_D(T)$ data than that of the leading order, (iii) $g_{\rm eff}(T)$ and $m_D(T)$ satisfy the leading-order formula, $m_D(T) = \sqrt{1 + N_f/6}\, g_{\rm eff}(T)T$ for $T > 1.5T_{\rm pc}$, so that most higher-order and nonperturbative effects on the Debye mass is likely to be absorbed in $g_{\rm eff}(T)$, and (iv) there is a quantitative discrepancy in $m_D(T)$ between our results using the Wilson quark action and those using the staggered quark action [12,13] even at $T \sim 4T_{\rm pc}$, and (v) the Casimir scaling law valid above $T_{\rm pc}$ is violated below $T_{\rm pc}$, in particular, in the color octet channel.

We also extract the spatial string tension σ_s at $T > T_{\rm pc}$ from the spatial Wilson loop. We show that $\sqrt{\sigma_s}$ has approximate linear increase with T, as previously reported in quenched studies [17–20]. We find that our result for σ_s agree quantitatively well with the analytic result based on a dimensionally reduced effective theory [21].

This paper is organized as follows: In Sec. II, we present our lattice action and simulation parameters, and discuss the line of constant physics. Results of numerical simulations for the heavy-quark free energies are shown in Sec. III. The effective running coupling and Debye screening mass are extracted from the heavy-quark free energies and are compared with the analytic results of thermal perturbation theory and with the numerical results with staggered quark action. The force between heavy quarks are also discussed in this section. In Sec. IV, we show the spatial string tension obtained from the spatial Wilson loop and its comparison to analytic results. The paper is concluded in Sec. V. We discuss the fit range dependence of the free energies in Appendix A, and tabulate numerical data of the free energies in Appendix B.

II. SIMULATIONS WITH A WILSON-TYPE QUARK ACTION

A. Lattice action

We employ the RG-improved gauge action [22] and the $N_f = 2$ clover-improved Wilson quark action [23] defined by

$$S = S_g + S_q, \tag{1}$$

$$S_g = -\beta \sum_x \Bigg(c_0 \sum_{\mu<\nu;\mu,\nu=1}^{4} W_{\mu\nu}^{1\times 1}(x) + c_1 \sum_{\mu\neq\nu;\mu,\nu=1}^{4} W_{\mu\nu}^{1\times 2}(x) \Bigg), \tag{2}$$

$$S_q = \sum_{f=1,2} \sum_{x,y} \bar{q}_x^f D_{x,y} q_y^f, \tag{3}$$

where $\beta = 6/g^2$, $c_1 = -0.331$, $c_0 = 1 - 8c_1$ and

$$D_{x,y} = \delta_{xy} - K \sum_\mu \{(1-\gamma_\mu) U_{x,\mu} \delta_{x+\hat{\mu},y} + (1+\gamma_\mu) U_{x,\mu}^\dagger \delta_{x,y+\hat{\mu}}\} - \delta_{xy} c_{\rm SW} K \sum_{\mu<\nu} \sigma_{\mu\nu} F_{\mu\nu}. \tag{4}$$

Here K is the hopping parameter and $F_{\mu\nu}$ is the lattice field strength, $F_{\mu\nu} = 1/8i(f_{\mu\nu} - f_{\mu\nu}^\dagger)$, with $f_{\mu\nu}$ the standard clover-shaped combination of gauge links. For the clover coefficient $c_{\rm SW}$, we adopt a mean field value using $W^{1\times 1}$ which was calculated in the one-loop perturbation theory [22],

$$c_{\rm SW} = (W^{1\times 1})^{-3/4} = (1 - 0.8412\beta^{-1})^{-3/4}. \tag{5}$$

The phase diagram of this action in the (β, K) plane has been obtained by the CP-PACS Collaboration [2,3] as shown in Fig. 1. The solid line $K_c(T = 0)$ with filled circles is the chiral limit where pseudoscalar mass vanishes at zero temperature. Above the $K_c(T = 0)$ line, the parity-flavor symmetry is spontaneously broken [24–26]. At finite temperatures, the cusp of the parity-broken phase retracts from the large β limit to a finite β [27,28]. The solid line $K_c(T > 0)$ connecting open symbols represents the boundary of the parity-broken phase. The region below K_c corresponds to the two-flavor QCD with finite quark mass. We perform simulations in this region after investigating the relation between the simulation parameters (β, K) and the physical parameters, e.g. quark mass and lattice spacing.

The dashed line K_t with filled diamond represents the finite temperature pseudocritical line determined from the peak of Polyakov loop susceptibility. This line separates the hot phase (the quark-gluon plasma phase) and the cold

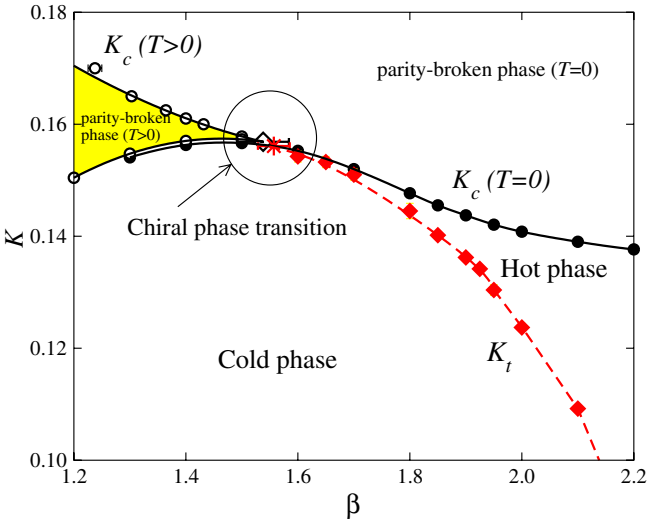

FIG. 1 (color online). Phase diagram for RG-improved gauge action and clover-improved Wilson quark action for $N_t = 4$.

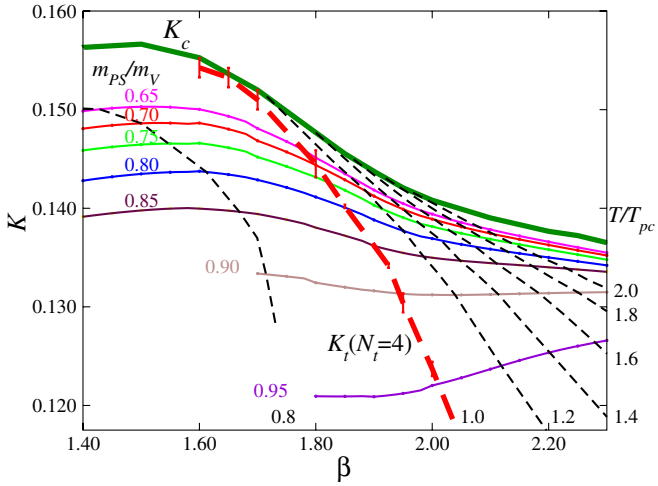

FIG. 3 (color online). Lines of constant $m_{\rm PS}/m_{\rm V}$ (solid lines) in the (β, K) plane for $m_{\rm PS}/m_{\rm V} = 0.65$, 0.70, 0.75, 0.80, 0.85, 0.90 and 0.95. Dashed lines represent lines of constant $T/T_{\rm pc}$ on $N_t = 4$ lattices, where $T_{\rm pc}$ is the pseudocritical temperature corresponding to $K_t(N_t = 4)$ shown by the thick solid line.

phase (the hadron phase). The crossing of the K_t and the $K_c(T = 0)$ lines is the chiral phase transition point.

B. Determination of lines of constant physics and simulation parameters

For phenomenological applications, we need to investigate the temperature dependence of thermodynamic observables on a line of constant physics (LCP), which we determine by $m_{\rm PS}/m_{\rm V}$ (the ratio of pseudoscalar and vector meson masses at $T = 0$). For our purpose, we need LCP in a wider range of parameters than that studied in Ref. [3]. Therefore, we reanalyze the data for $m_{\rm PS}a$ and $m_{\rm V}a$ at zero temperature in a wider range shown in Fig. 2, where a is the lattice spacing [2,3,7,8]. The thin solid lines in Fig. 3 shows our results for LCP corresponding to $m_{\rm PS}/m_{\rm V} =$ 0.65, 0.70, 0.75, 0.80, 0.85, 0.90 and 0.95. The bold solid line denoted as K_c represents the critical line, i.e. $m_{\rm PS}/m_{\rm V} = 0$. Our LCP's are consistent with those of [3] in the range of the previous study.

We also reanalyze the lines of constant $T/T_{\rm pc}$. The temperature T is estimated by the zero-temperature vector meson mass $m_{\rm V}a(\beta, K)$ using

$$\frac{T}{m_{\rm V}}(\beta, K) = \frac{1}{N_t \times m_{\rm V}a(\beta, K)}. \qquad (6)$$

The lines of constant $T/T_{\rm pc}$ is determined by the ratio of $T/m_{\rm V}$ to $T_{\rm pc}/m_{\rm V}$ where $T_{\rm pc}/m_{\rm V}$ is obtained by $T/m_{\rm V}$ at K_t on the same LCP. We use an interpolation function, $T_{\rm pc}/m_{\rm V} = A(1 + B(m_{\rm PS}/m_{\rm V})^2)/(1 + C(m_{\rm PS}/m_{\rm V})^2)$ with $A = 0.2253(71)$, $B = -0.933(17)$ and $C = -0.820(39)$, obtained in Ref. [3] to evaluate $T_{\rm pc}/m_{\rm V}$ for each

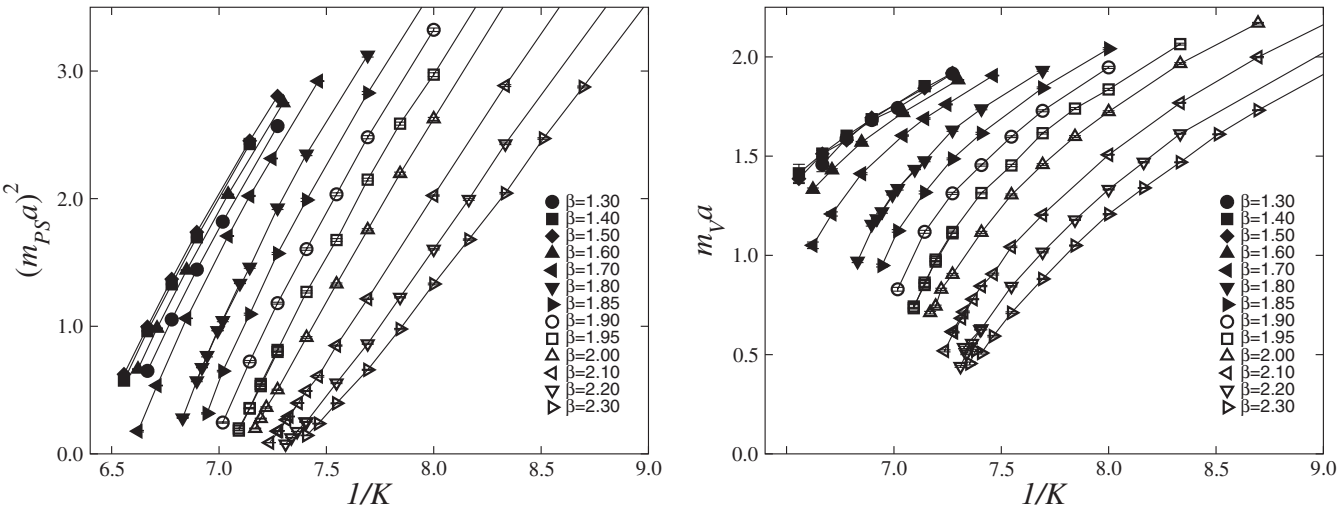

FIG. 2. Pseudoscalar meson mass squared (left) and vector meson mass (right) as a function of $1/K$ for several values of β at $T = 0$.

TABLE I. Simulation parameters for $m_{\rm PS}/m_{\rm V} = 0.65$ (left) and $m_{\rm PS}/m_{\rm V} = 0.80$ (right).

β	K	$T/T_{\rm pc}$	Traj.
1.50	0.150290	0.82(3)	5000
1.60	0.150030	0.86(3)	5000
1.70	0.148086	0.94(3)	5000
1.75	0.146763	1.00(4)	5000
1.80	0.145127	1.07(4)	5000
1.85	0.143502	1.18(4)	5000
1.90	0.141849	1.32(5)	5000
1.95	0.140472	1.48(5)	5000
2.00	0.139411	1.67(6)	5000
2.10	0.137833	2.09(7)	5000
2.20	0.136596	2.59(9)	5000
2.30	0.135492	3.22(12)	5000
2.40	0.134453	4.02(15)	5000

β	K	$T/T_{\rm pc}$	Traj.
1.50	0.143480	0.76(4)	5500
1.60	0.143749	0.80(4)	6000
1.70	0.142871	0.84(4)	6000
1.80	0.141139	0.93(5)	6000
1.85	0.140070	0.99(5)	6000
1.90	0.138817	1.08(5)	6000
1.95	0.137716	1.20(6)	6000
2.00	0.136931	1.35(7)	5000
2.10	0.135860	1.69(8)	5000
2.20	0.135010	2.07(10)	5000
2.30	0.134194	2.51(13)	5000
2.40	0.133395	3.01(15)	5000

$m_{\rm PS}/m_{\rm V}$. The bold dashed line denoted as $K_t(N_t = 4)$ in Fig. 3 represents the pseudocritical line $T/T_{\rm pc} = 1$. The thin dashed lines represent the results for $T/T_{\rm pc} = 0.8$, 1.2, 1.4, 1.6, 1.8, 2.0 at $N_t = 4$.

We perform finite temperature simulations on a lattice with a temporal extent $N_t = 4$ and a spatial extent $N_s = 16$ along the LCP's for $m_{\rm PS}/m_{\rm V} = 0.65$ and 0.80. The standard hybrid Monte Carlo algorithm is employed to generate full QCD configurations with two flavors of dynamical quarks. The length of one trajectory is unity and the step size of the molecular dynamics is tuned to achieve an acceptance rate greater than 70%. Runs are carried out in the range $\beta = 1.50$–2.40 at 13 values of $T/T_{\rm pc} \sim 0.82$–4.0 for $m_{\rm PS}/m_{\rm V} = 0.65$ and 12 values of $T/T_{\rm pc} \sim 0.76$–3.0 for $m_{\rm PS}/m_{\rm V} = 0.80$. Our simulation parameters and the corresponding temperatures are summarized in Table I. Because the determination of the pseudocritical line is more difficult than the calculation of $T/m_{\rm V}$, the dominant source for the error of $T/T_{\rm pc}$ in Table I is the overall factor $T_{\rm pc}/m_{\rm V}$. The number of trajectories for each run after thermalization is 5000–6000. We measure physical quantities at every 10 trajectories.

III. HEAVY-QUARK FREE ENERGIES

A free energy of static quarks on the lattice is described by the correlations of the Polyakov loop: $\Omega(\mathbf{x}) = \prod_{\tau=1}^{N_t} U_4(\tau, \mathbf{x})$ where the $U_\mu(\tau, \mathbf{x}) \in {\rm SU}(3)$ is the link variable. With an appropriate gauge fixing, one can define the free energy in various color channels separately [29,30]: the color singlet $Q\bar{Q}$ channel (**1**), the color octet $Q\bar{Q}$ channel (**8**), the color antitriplet QQ channel (**3***), and the color sextet QQ channel (**6**), given as follows:

$$e^{-F_{\mathbf{1}}(r,T)/T} = \tfrac{1}{3}\langle {\rm Tr}\Omega^\dagger(\mathbf{x})\Omega(\mathbf{y})\rangle, \tag{7}$$

$$e^{-F_{\mathbf{8}}(r,T)/T} = \tfrac{1}{8}\langle {\rm Tr}\Omega^\dagger(\mathbf{x})\,{\rm Tr}\Omega(\mathbf{y})\rangle - \tfrac{1}{24}\langle {\rm Tr}\Omega^\dagger(\mathbf{x})\Omega(\mathbf{y})\rangle, \tag{8}$$

$$e^{-F_{\mathbf{6}}(r,T)/T} = \tfrac{1}{12}\langle {\rm Tr}\Omega(\mathbf{x})\,{\rm Tr}\Omega(\mathbf{y})\rangle + \tfrac{1}{12}\langle {\rm Tr}\Omega(\mathbf{x})\Omega(\mathbf{y})\rangle, \tag{9}$$

$$e^{-F_{\mathbf{3}^*}(r,T)/T} = \tfrac{1}{6}\langle {\rm Tr}\Omega(\mathbf{x})\,{\rm Tr}\Omega(\mathbf{y})\rangle - \tfrac{1}{6}\langle {\rm Tr}\Omega(\mathbf{x})\Omega(\mathbf{y})\rangle, \tag{10}$$

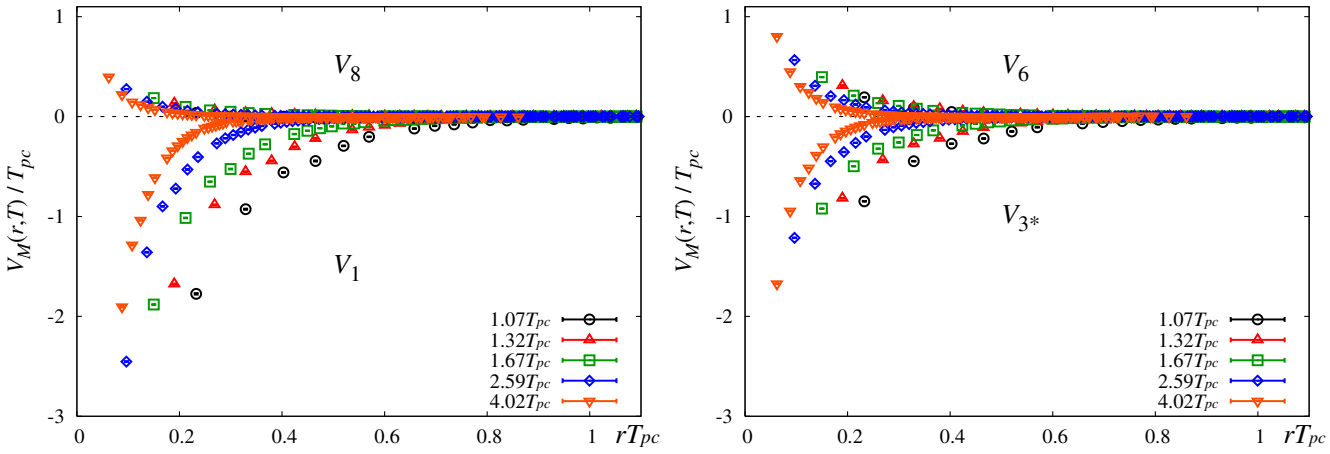

FIG. 4 (color online). Simulation results of the normalized free energies scaled by $T_{\rm pc}$ for color-singlet and octet $Q\bar{Q}$ channels (left) and color antitriplet and sextet QQ channels (right) at $m_{\rm PS}/m_{\rm V} = 0.65$.

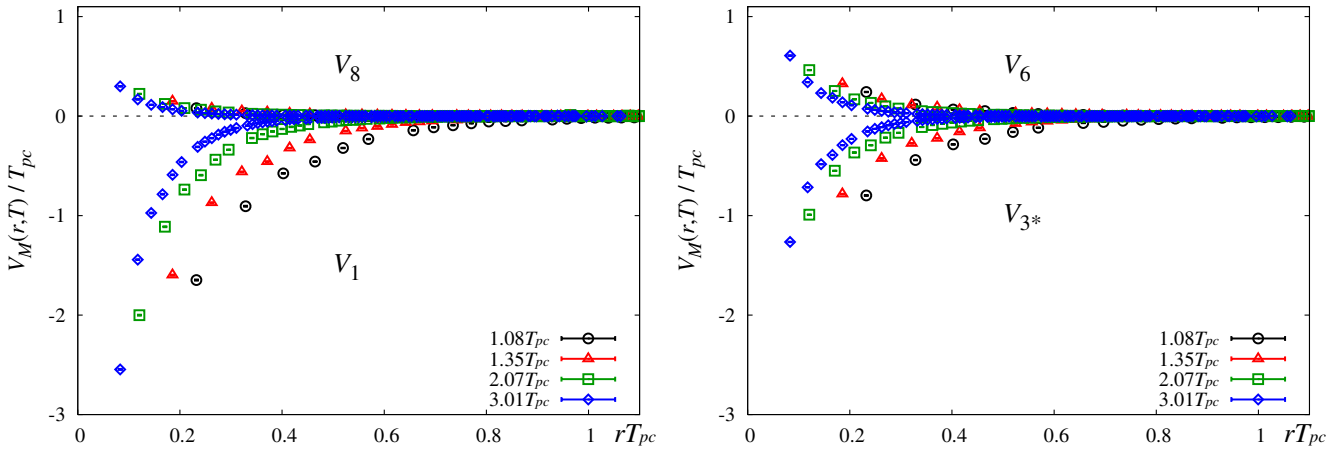

FIG. 5 (color online). The same figure with Fig. 4 at $m_{\rm PS}/m_{\rm V} = 0.80$.

where $r = |\mathbf{x} - \mathbf{y}|$. We adopt the Coulomb gauge fixing in this study.

Above $T_{\rm pc}$, we introduce normalized free energies ($V_{\mathbf{1}}$, $V_{\mathbf{8}}$, $V_{\mathbf{6}}$, $V_{\mathbf{3}^*}$) such that they vanish at large distances. This is equivalent to defining the free energies by dividing the right-hand sides of Eqs. (7)–(10) by $\langle {\rm Tr}\Omega\rangle^2$.

The normalized free energies are shown in Fig. 4 for color-singlet and octet $Q\bar{Q}$ channels (left) and color antitriplet and sextet QQ channels (right) for $m_{\rm PS}/m_{\rm V} = 0.65$ and $T \geq T_{\rm pc}$. These for $m_{\rm PS}/m_{\rm V} = 0.80$ are also shown in Fig. 5. Data of the normalized free energies for all temperatures above $T_{\rm pc}$ are summarized in Tables V, VI, VII, VIII, IX, X, XI, XII, and XIII of Appendix B. From these figures, we find that the interquark interaction is ''attractive'' in the color-singlet and antitriplet channels and is ''repulsive'' in the color octet and sextet channels. We also see that, irrespective of the channels, the interquark interaction becomes rapidly weak at long distances as T increases, as expected from the Debye screening at high temperatures. These behaviors are qualitatively similar to the case of quenched QCD in the Lorenz gauge as reported in Ref. [10,11].

To study the screening effects in each color channel more closely, we fit the free energies by the screened Coulomb form

$$V_M(r,T) = C(M)\frac{\alpha_{\rm eff}(T)}{r}e^{-m_D(T)r}, \qquad (11)$$

where $\alpha_{\rm eff}(T)$ and $m_D(T)$ are the effective running coupling and Debye screening mass, respectively. The Casimir factor $C(M) \equiv \langle \sum_{a=1}^{8} t_1^a \cdot t_2^a \rangle_M$ for color channel M is explicitly given by

$$C(\mathbf{1}) = -\tfrac{4}{3}, \quad C(\mathbf{8}) = \tfrac{1}{6}, \quad C(\mathbf{6}) = \tfrac{1}{3}, \quad C(\mathbf{3}^*) = -\tfrac{2}{3}, \qquad (12)$$

for our cases. Here, it is worth stressing that, with the improved actions we adopt, the rotational symmetry is well restored in the heavy-quark free energies [31]. Therefore, we do not need to introduce terms correcting lattice artifacts at short distances in Eq. (11) to fit the data shown in Fig. 4 and 5.

The Debye screening effect is defined through the long distance behavior of $V_M(r,T)$. A discussion to determine an appropriate fit range is given in Appendix A and we choose it to be $\sqrt{11}/4 \leq rT \leq 1.5$. We also discuss the systematic errors due to a difference of the fit ranges in Appendix A, and find that the systematic errors are smaller than the statistical errors at $T \gtrsim 2T_{\rm pc}$. The fit is performed by minimizing χ^2/N_{DF}, where $N_{DF} = 20$. Results of the χ^2/N_{DF} for each color channel and temperature are summarized in Table II for $m_{\rm PS}/m_{\rm V} = 0.65$ (left) and 0.80 (right).

TABLE II. The χ^2/N_{DF} for each color channel and temperature at $m_{\rm PS}/m_{\rm V} = 0.65$ (left) and 0.80 (right).

$T/T_{\rm pc}$	$M = \mathbf{1}$	$\mathbf{8}$	$\mathbf{6}$	$\mathbf{3}^*$
1.00	1.97	2.26	2.50	1.41
1.07	2.06	0.99	1.04	1.59
1.18	2.08	1.86	1.21	1.59
1.32	1.19	4.02	1.58	0.85
1.48	1.32	1.55	1.06	0.98
1.67	2.96	1.65	1.98	2.64
2.09	3.51	2.16	2.07	1.64
2.59	1.49	0.98	1.25	3.55
3.22	2.05	1.66	2.14	1.83
4.02	2.75	1.51	1.37	2.73

$T/T_{\rm pc}$	$M = \mathbf{1}$	$\mathbf{8}$	$\mathbf{6}$	$\mathbf{3}^*$
1.08	1.25	1.14	[a]	0.82
1.20	1.78	1.66	1.33	0.95
1.35	1.32	0.76	2.10	0.81
1.69	1.01	1.58	1.07	1.22
2.07	4.07	1.51	2.28	2.80
2.51	2.00	2.72	1.43	1.93
3.01	2.13	2.60	1.56	2.08

[a]Fit is unstable since $V_{\mathbf{6}}(r,T)$ at this parameter point is smaller than the statistical errors in the fit range.

The results of $\alpha_{\rm eff}(T)$ and $m_D(T)$ are shown in Fig. 6 for $m_{\rm PS}/m_{\rm V} = 0.65$ and Fig. 7 for 0.80. The numerical results are also summarized in Table III for $m_{\rm PS}/m_{\rm V} = 0.65$ and Table IV for 0.80. We find that there is no significant channel dependence in $\alpha_{\rm eff}(T)$ and $m_D(T)$ at sufficiently high temperatures ($T \gtrsim 2T_{\rm pc}$). In other words, the channel

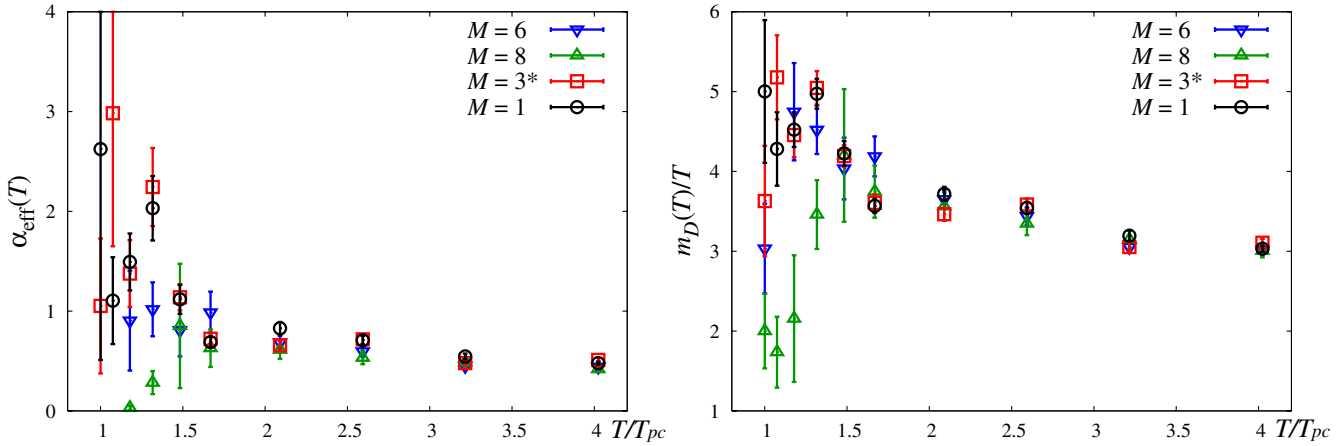

FIG. 6 (color online). The effective running coupling $\alpha_{\rm eff}(T)$ (left) and Debye screening mass $m_D(T)$ (right) for each color channel as a function of temperature from the large distance behavior of the potentials at $m_{\rm PS}/m_{\rm V} = 0.65$.

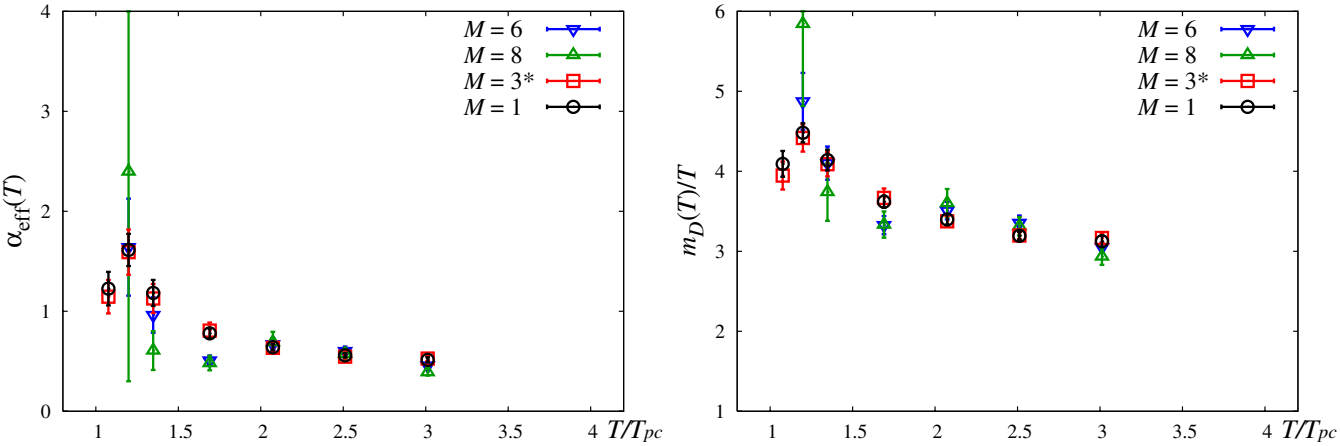

FIG. 7 (color online). The same figures with Fig. 6 at $m_{\rm PS}/m_{\rm V} = 0.80$.

TABLE III. Results of $\alpha_{\rm eff}(T)$ and $m_D(T)$ at $m_{\rm PS}/m_{\rm V} = 0.65$ with statistical errors determined by a jackknife method with the bin-size of 100 trajectories.

	$\alpha_{\rm eff}(T)$				$m_D(T)$			
$T/T_{\rm pc}$	$M = \mathbf{1}$	**8**	**6**	$\mathbf{3}^*$	**1**	**8**	**6**	$\mathbf{3}^*$
1.00	2.62(211)	−0.47(21)	−0.60(31)	1.05(67)	5.00(89)	2.00(46)	3.03(56)	3.63(69)
1.07	1.11(43)	−0.17(6)	−0.01(0)	2.98(133)	4.28(46)	1.74(44)	0.09(40)	5.18(52)
1.18	1.49(28)	0.03(2)	0.90(50)	1.38(33)	4.52(21)	2.16(79)	4.75(60)	4.46(27)
1.32	2.03(32)	0.28(11)	1.02(27)	2.24(39)	4.97(18)	3.46(43)	4.52(30)	5.05(21)
1.48	1.12(14)	0.85(62)	0.81(26)	1.14(13)	4.23(15)	4.20(83)	4.04(38)	4.19(13)
1.67	0.69(5)	0.63(18)	0.99(20)	0.72(6)	3.57(8)	3.75(32)	4.19(25)	3.61(10)
2.09	0.83(6)	0.61(9)	0.69(6)	0.66(4)	3.72(8)	3.56(17)	3.65(11)	3.46(8)
2.59	0.71(4)	0.53(6)	0.60(5)	0.72(4)	3.54(7)	3.35(14)	3.44(10)	3.59(7)
3.22	0.55(2)	0.49(5)	0.45(2)	0.48(2)	3.19(6)	3.15(11)	3.05(6)	3.05(5)
4.02	0.48(1)	0.42(2)	0.44(1)	0.51(2)	3.03(3)	3.01(8)	3.02(5)	3.11(4)

TABLE IV. The same Table as Table III at $m_{\rm PS}/m_{\rm V} = 0.80$.

	$\alpha_{\rm eff}(T)$				$m_D(T)$			
$T/T_{\rm pc}$	$M = \mathbf{1}$	**8**	**6**	**3***	**1**	**8**	**6**	**3***
1.08	1.23(16)	−0.03(1)	···	1.15(16)	4.09(16)	0.63(39)	···	3.95(17)
1.20	1.61(16)	2.40(209)	1.64(48)	1.59(22)	4.48(12)	5.84(102)	4.87(35)	4.42(17)
1.35	1.18(12)	0.61(19)	0.96(17)	1.13(14)	4.14(12)	3.74(36)	4.10(20)	4.09(15)
1.69	0.78(4)	0.48(7)	0.51(5)	0.81(8)	3.62(7)	3.33(16)	3.33(11)	3.67(11)
2.07	0.64(3)	0.69(10)	0.67(6)	0.63(3)	3.40(6)	3.60(17)	3.51(10)	3.37(6)
2.51	0.56(2)	0.57(5)	0.60(4)	0.55(1)	3.19(4)	3.31(11)	3.36(9)	3.20(4)
3.01	0.51(2)	0.39(3)	0.46(2)	0.53(2)	3.13(6)	2.93(10)	3.05(5)	3.17(6)

dependence in the free energy can be well absorbed in the kinematical Casimir factor at high temperatures, as first indicated in quenched studies [10,11].

A. Debye mass on the lattice and that in perturbative theory

Let us first compare the Debye mass on the lattice with that calculated in the thermal perturbation theory. The 2-loop running coupling is given by

$$g_{2\rm l}^{-2}(\mu) = \beta_0 \ln\left(\frac{\mu}{\Lambda}\right)^2 + \frac{\beta_1}{\beta_0}\ln\ln\left(\frac{\mu}{\Lambda}\right)^2, \qquad (13)$$

where the argument in the logarithms can be written as $\mu/\Lambda = (\mu/T)(T/T_{\rm pc})(T_{\rm pc}/\Lambda)$ where we adopt $\Lambda = \Lambda_{\overline{\rm MS}}^{N_f=2} \simeq 261$ MeV [32] and $T_{\rm pc} \simeq 171$ MeV [2]. We assume that the renormalization point μ is in the range $\mu = \pi T$ to $3\pi T$. Therefore, $g_{2\rm l}$ can be viewed as a function of $T/T_{\rm pc}$. With $g_{2\rm l}$, the Debye screening mass is given by

$$\frac{m_D^{\rm LO}(T)}{T} = \sqrt{1 + \frac{N_f}{6}}\, g_{2\rm l}(\mu), \qquad (14)$$

in the leading-order (LO) thermal perturbation theory, neglecting the effects of quark masses.

In Fig. 8 (left) we compare $m_D(T)$ in the color-singlet channel with $m_D^{\rm LO}(T)/T$ for $\mu = \pi T$, $2\pi T$ and $3\pi T$. We find that the leading-order screening mass $m_D^{\rm LO}(T)$ does not reproduce the simulation results at all. Similar discrepancy has been observed also in quenched QCD [33] and in full QCD with staggered quarks [12].

To study higher-order contributions in the thermal perturbation theory, we test the Debye mass in the next-to-leading-order calculated by the hard thermal loop resummation method [34],

$$\frac{m_D^{\rm NLO}(T)}{T} = \sqrt{1 + \frac{N_f}{6}}\, g_{2\rm l}(\mu)\Bigg[1 + g_{2\rm l}(\mu)\frac{3}{2\pi} \times \sqrt{\frac{1}{1 + N_f/6}}\left(\ln\frac{2m_D^{\rm LO}}{m_{\rm mag}} - \frac{1}{2}\right) + \mathcal{O}(g^2)\Bigg]. \qquad (15)$$

Here $m_{\rm mag}(T) = C_m g_{2\rm l}^2(\mu) T$ denotes the magnetic screening mass. The factor C_m cannot be determined within the perturbation theory due to the infrared problem. In this study, we adopt $C_m \simeq 0.482$ obtained by a quenched lattice

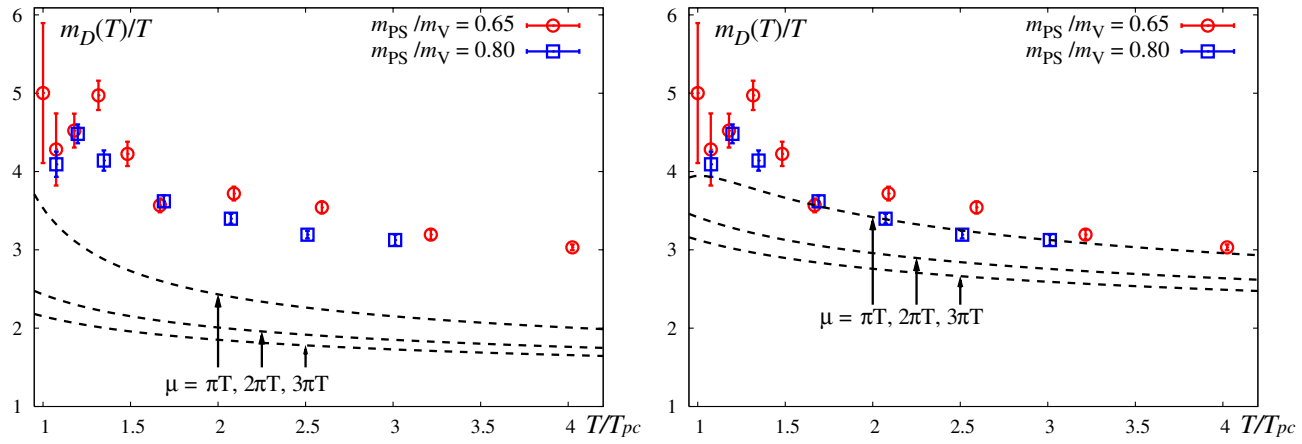

FIG. 8 (color online). The Debye screening masses $m_D(T)$ at $m_{\rm PS}/m_{\rm V} = 0.65$ and 0.80 in the color-singlet channel together with that calculated in the leading-order (left) and next-to-leading-order (right) thermal perturbation theory shown by the dashed lines. μ is the renormalization point chosen at $\mu = \pi T$, $2\pi T$, $3\pi T$.

simulation [33] as a typical value.[1] In Fig. 8 (right), our simulation results for m_D are compared with $m_D^{\mathrm{NLO}}(T)$ shown by the dashed lines. The values of m_D^{NLO} are larger than m_D^{LO} by approximately 50% and agree better with the simulation results.

B. Phenomenological relation between α_{eff} and m_D

So far, we have fitted the free energies on the lattice treating α_{eff} and m_D as independent parameters. In this subsection, we test an ansatz inspired from the leading-order perturbation theory:

$$\frac{m_D(T)}{T} = \sqrt{1 + \frac{N_f}{6}}\, g_{\mathrm{eff}}(T), \tag{16}$$

with $g_{\mathrm{eff}}(T) \equiv \sqrt{4\pi\alpha_{\mathrm{eff}}(T)}$. Therefore, if this relation holds, we expect that the ratio

$$R(T) \equiv \frac{(1 + N_f/6)^{-1/2} m_D(T)/T}{\sqrt{4\pi\alpha_{\mathrm{eff}}(T)}}, \tag{17}$$

should be close to unity ($R(T) \sim 1$).

In Fig. 9, our simulation results of $R(T)$ for the singlet channel are shown as a function of T/T_{pc}. We find that $R(T)$ is consistent with unity for $T \gtrsim 1.5T_{\mathrm{pc}}$ within 10% accuracy. This is a nontrivial observation particularly near T_{pc} and suggests that the major part of the higher-order effects and nonperturbative effects of $m_D(T)$ can be expressed by the effective running coupling $g_{\mathrm{eff}}(T)$. We note that a similar effective coupling at $T = 0$ defined through the lattice potential was introduced to improve the lattice perturbation theory [35].

C. Comparison with the staggered quark action

Finally, we compare the results of $\alpha_{\mathrm{eff}}(T)$ and $m_D(T)$ obtained by the Wilson quark action (present work) with those by an improved staggered quark action on a $16^3 \times 4$ lattice at $m_{\mathrm{PS}}/m_{\mathrm{V}} \simeq 0.70$ [12,13]. The comparison is shown in Fig. 10 for $\alpha_{\mathrm{eff}}(T)$ (left panel) and $m_D(T)$ (right panel). Although $\alpha_{\mathrm{eff}}(T)$ does not show significant difference between the two actions, $m_D(T)$ in the Wilson quark action is systematically higher than that of the staggered quark action by about 20% even at $T = 4T_{\mathrm{pc}}$. This discrepancy can be seen directly from the normalized free energies in Fig. 11 where $-r \times V_{\mathbf{1}}(r)$ is shown as a function of rT at $T \simeq 1.7T_{\mathrm{pc}}$ (left) and $\simeq 4.0T_{\mathrm{pc}}$ (right). The circles (triangles) are the results of the Wilson quark action (staggered quark action). The data for the staggered quark action is taken from Ref. [12]. The straight lines are the fits

[1]When we fit C_m from our simulation results $m_D(T = 4.02T_{\mathrm{pc}})$ with $\mu = 2\pi T$, we obtain $C_m \simeq 0.33$.

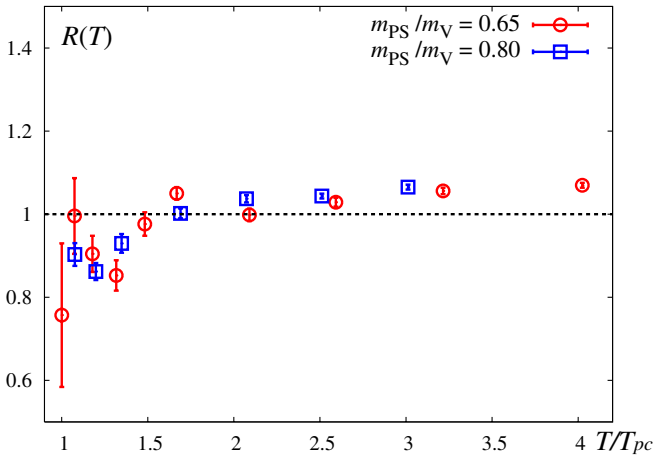

FIG. 9 (color online). The ratio $R(T)$ in the text which is supposed to be close to unity if $m_D(T) = \sqrt{1 + N_f/6}\, g_{\mathrm{eff}}(T)T$ holds. The results are for the color-singlet channel.

with the screened Coulomb form, Eq. (11), in the range $\sqrt{11}/4 \le rT \le 1.5$ (circles) and 0.8–1.0 $\lesssim rT$ (triangles). The intercepts of the lines with the vertical axis and the slopes of the lines correspond to $\alpha_{\mathrm{eff}}(T)$ and $m_D(T)$, respectively. There is an obvious difference in the slope in different quark actions, which may be regarded as systematic errors due to the lattice discretization. This discrepancy should be further investigated at smaller lattice spacing, i.e. larger lattice size in the temporal direction.

D. Force between heavy quarks

To make a direct comparison of the free energies below and above T_{pc}, we study the "force" between heavy quarks defined by $dF_M(r, T)/dr$ without introducing the subtraction of $\langle \mathrm{Tr}\Omega \rangle^2$. In Fig. 12, such forces are shown for color-singlet (left) and octet (right) $Q\bar{Q}$ channels, and in Fig. 13, for color sextet (left) and antitriplet (right) QQ channels at $m_{\mathrm{PS}}/m_{\mathrm{V}} = 0.65$. Results at $m_{\mathrm{PS}}/m_{\mathrm{V}} = 0.80$ are shown in Fig. 14 and 15.

In the color-singlet and antitriplet channels, there is always an "attraction" both for $T < T_{\mathrm{pc}}$ and for $T > T_{\mathrm{pc}}$, and the "attraction" is stronger as we decrease the temperature. The signal for the color sextet channel below T_{pc} is rather weak and we cannot make a definite statement from our data. On the other hand, the force in the color octet channel is clearly "attractive" ("repulsive") at low (high) T. Namely, the simple Casimir scaling law, which worked well at high T, does not hold below T_{pc}. In Ref. [36], it has be suggested that the Polyakov loop correlation in the octet channel is saturated by the color-singlet intermediate states at very low temperature. If this is true, the attraction in the color octet channel found here is explained by the attraction in the singlet channel.

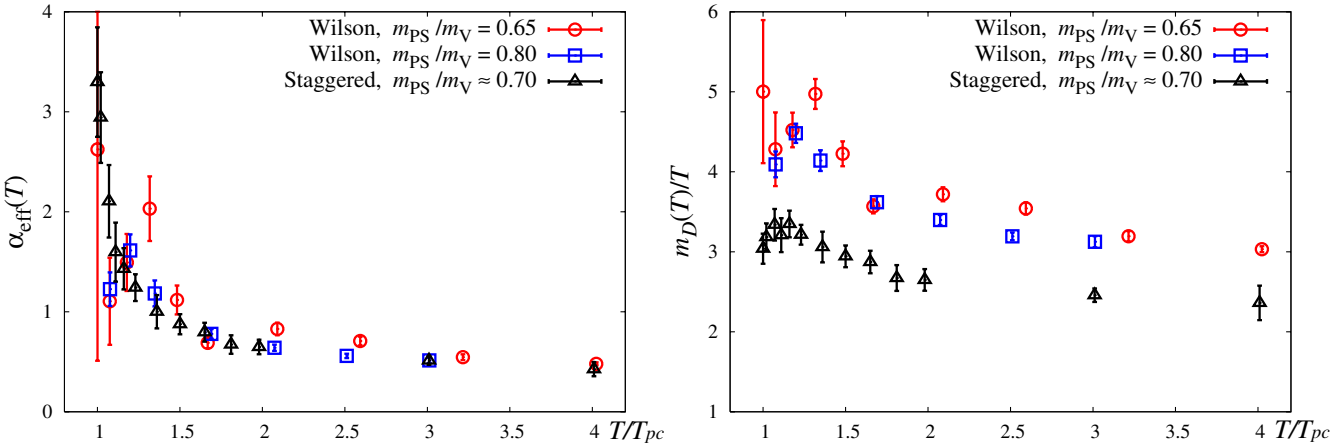

FIG. 10 (color online). Comparison of the $\alpha_{\rm eff}(T)$ (left) and $m_D(T)$ (right) between the results of the Wilson quark action and staggered quark action.

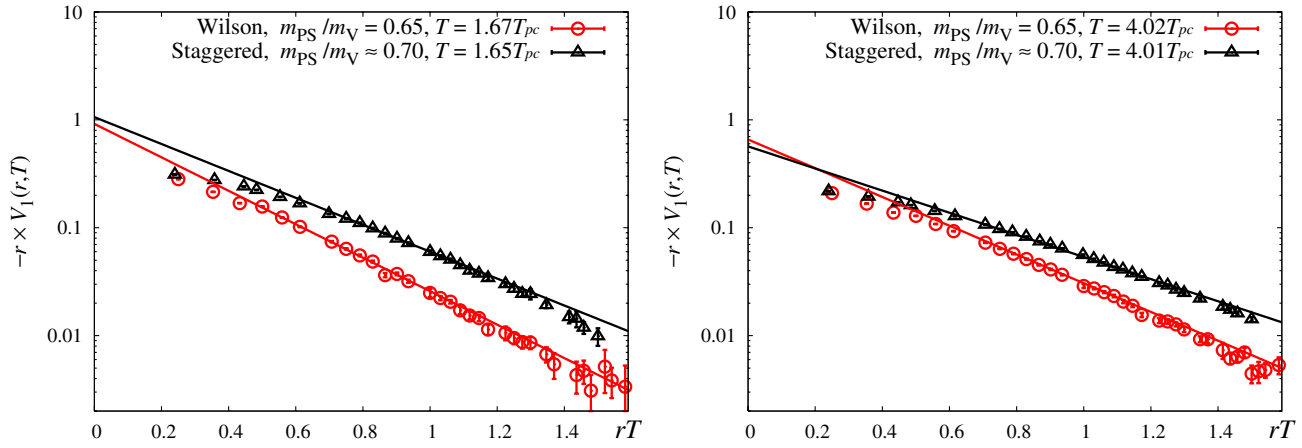

FIG. 11 (color online). Comparison of the normalized free energies, $-r \times V_1(r)$, between the Wilson quark action (present work) and the staggered quark action in Ref. [12] as a function of rT at $T \simeq 1.7T_{\rm pc}$ (left) and $\simeq 4.0T_{\rm pc}$ (right) with the log scale. Straight lines show the fits based on the screened Coulomb form in the range $\sqrt{11}/4 \leq rT \leq 1.5$ (circles) and 0.8–1.0 $\lesssim rT$ (triangles).

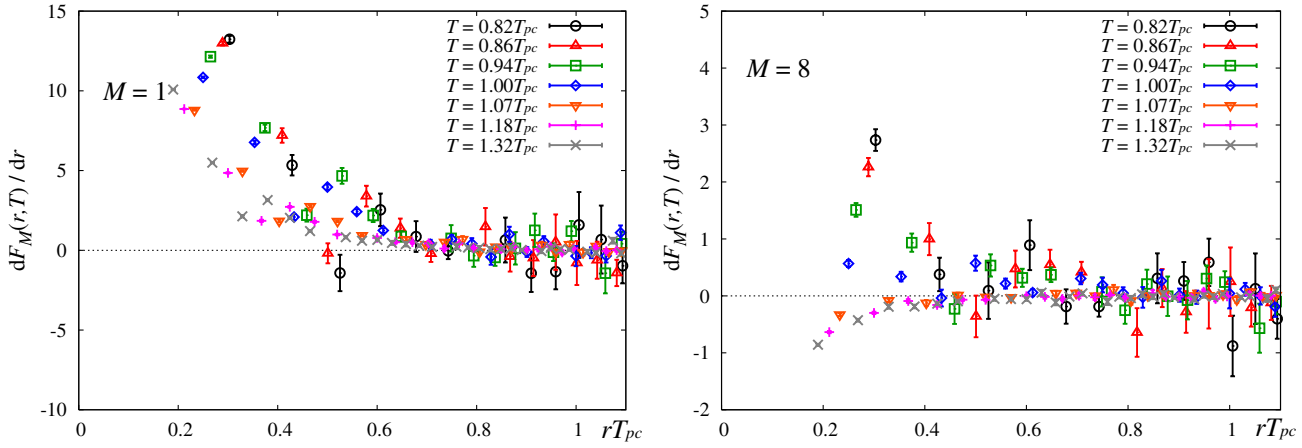

FIG. 12 (color online). Results of $dF_M(r)/dr$ scaled by $T_{\rm pc}$ for color-singlet (left) and octet (right) $Q\bar{Q}$ channels at $m_{\rm PS}/m_{\rm V} = 0.65$.

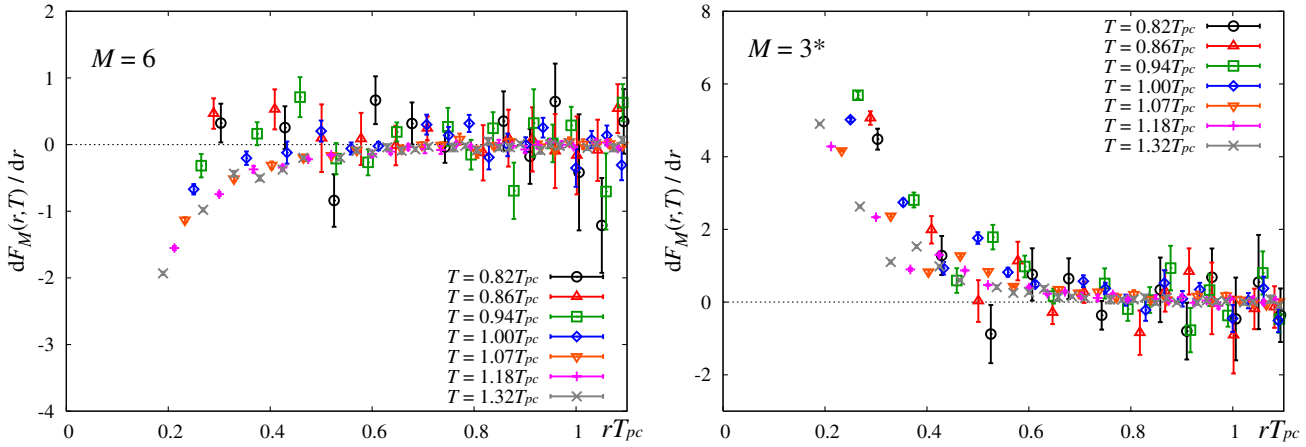

FIG. 13 (color online). Results of $dF_M(r)/dr$ scaled by $T_{\rm pc}$ for color sextet (left) and antitriplet (right) QQ channels at $m_{\rm PS}/m_{\rm V} = 0.65$.

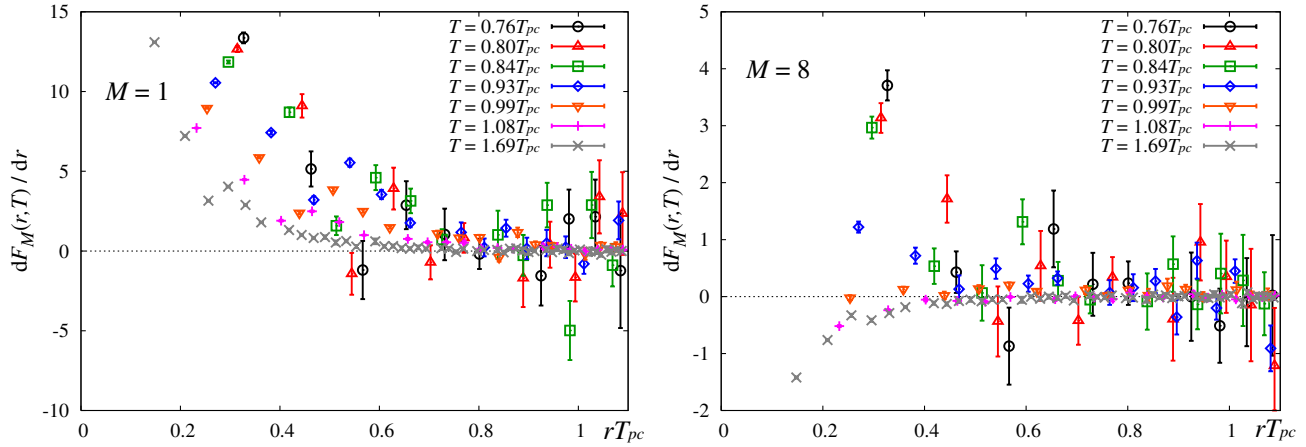

FIG. 14 (color online). The same as Fig. 12 at $m_{\rm PS}/m_{\rm V} = 0.80$.

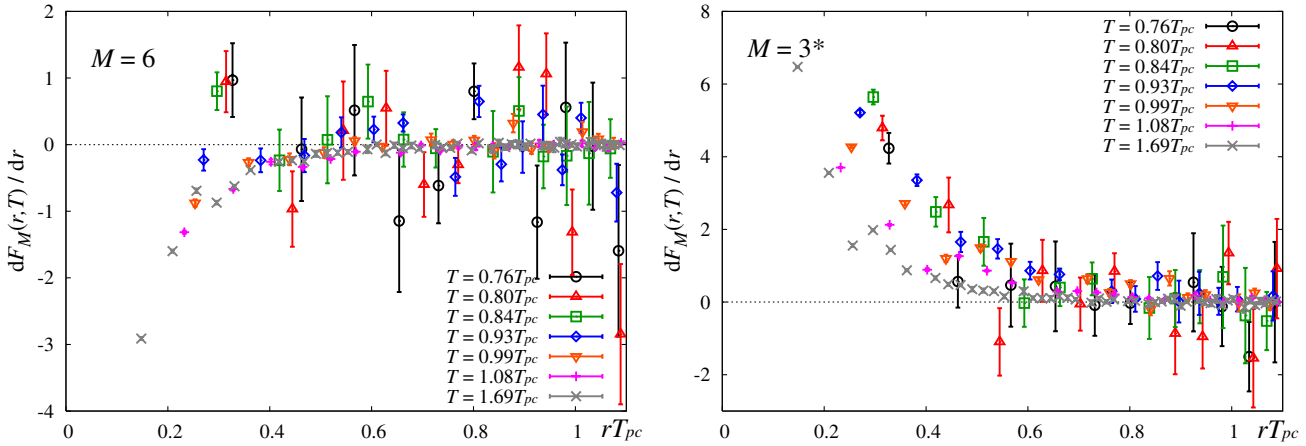

FIG. 15 (color online). The same as Fig. 13 at $m_{\rm PS}/m_{\rm V} = 0.80$.

IV. SPATIAL WILSON LOOP

In previous quenched studies [17–20], the Wilson loop in spatial direction is found to show nonvanishing spatial string tension σ_s even at $T > T_{\rm pc}$, which is called the spatial confinement. We study this phenomenon with the existence of dynamical quarks in the system. Although quarks are expected to decouple from the spatial observables for $T \gg T_{\rm pc}$ due to dimensional reduction and thus do not affect σ_s in the high temperature limit, it is not obvious whether the same is true near $T_{\rm pc}$.

We evaluate σ_s assuming a simplest ansatz for the spatial Wilson loop $W(I, J)$ with the size $I \times J$:

$$-\ln W(I, J) = \sigma_s IJ + \sigma_p(2I + 2J) + C_w, \tag{18}$$

where σ_s, σ_p and C_w are fit parameters. The results of $\sqrt{\sigma_s(T)}/T_{\rm pc}$ are shown in Fig. 16 (left) as a function of $T/T_{\rm pc}$. We find that $\sqrt{\sigma_s(T)}/T_{\rm pc}$ approaches to a constant as T decreases below $T_{\rm pc}$, while it increases linearly as T above $T_{\rm pc}$. Similar behavior has been observed in the quenched case [17].

Let us first make a phenomenological parametrization of the spatial string tension

$$\sqrt{\sigma_s(T)} = c g_{2l}^2(\mu) T, \tag{19}$$

motivated by the dimensional reduction at high temperature with $g_{2l}^2(\mu)$ being the two-loop running coupling of two-flavor QCD defined in Eq. (13). Our results for $\sqrt{\sigma_s(T)}/T$ are shown in Fig. 16 (right). The solid and dashed lines in the figure are the results of a fit of our data in the range $T > 1.3T_{\rm pc}$ to the formula Eq. (19). Here, we fix $\mu = 2\pi T$ and take c and $\Lambda/T_{\rm pc}$ as fitting parameters to obtain

$$c = 0.694(12), \qquad \Lambda/T_{\rm pc} = 0.866(48) \quad \text{for } m_{\rm PS}/m_{\rm V} = 0.65, \tag{20}$$

$$c = 0.639(34), \qquad \Lambda/T_{\rm pc} = 0.92(14) \quad \text{for } m_{\rm PS}/m_{\rm V} = 0.80. \tag{21}$$

Similar numbers have been observed in a quenched simulation [20], $(c, \Lambda/T_{\rm pc}) = (0.566(13), 0.653(57))$, and in a $2+1$ flavor simulation with staggered quark [37], $(c, \Lambda/T_{\rm pc}) = (0.587(41), 0.72(17))$. (Here we rescaled the previous results of Λ by 2π to compare at the common value of $\mu = 2\pi T$.)

Let us now make an alternative comparison of our data with a recent prediction by the parameter-free three-dimensional ($3d$) effective theory [21,38], which gives

$$\sqrt{\sigma_s} = 0.553(1) g_{\rm M}^2, \tag{22}$$

where the coefficient 0.553(1) expresses a nonperturbative contribution determined by $3d$ quenched lattice simulations, and $g_{\rm M}$ is a dimensionful $3d$ gauge coupling defined through the four-dimensional running coupling, $g(\mu)$, as

$$g_{\rm M}^2 = g_{2l}^2(\mu) T[1 + C_1 g_{2l}^2(\mu) + C_2 g_{2l}^4(\mu) + \cdots]. \tag{23}$$

Known coefficients C_1 and C_2 represent the next-to-leading (NLO) and next-to-next-leading (NNLO) contributions in $3d$ effective theory [21]. We choose $\mu/T = 2\pi$, which is in the range 6.0–7.0 assumed in the study of Ref. [21]. We take the same value for $\Lambda/T_{\rm pc} = \Lambda_{\overline{\rm MS}}^{N_f=2}/T_{\rm pc}$ as that in Sec. III A.

Figure 17 shows the results of the spatial string tension, together with the prediction from the $3d$ effective theory in the leading order, NLO and NNLO. We observe that convergence of the series is rather well and the NNLO result is

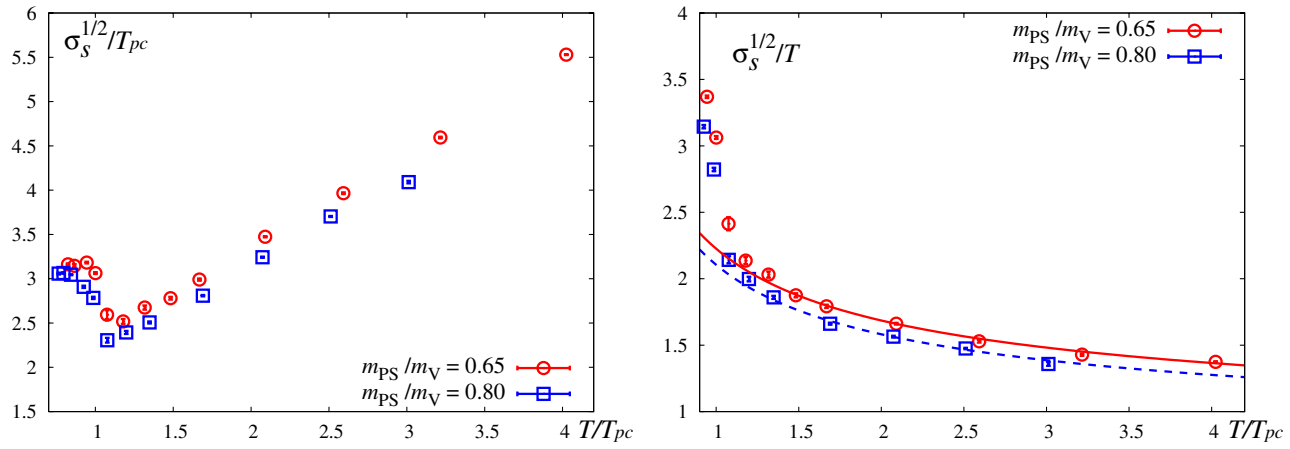

FIG. 16 (color online). The square root of the spatial string tension over $T_{\rm pc}$ (left) and T (right) as a function of $T/T_{\rm pc}$ at $m_{\rm PS}/m_{\rm V} = 0.65$ and 0.80. The solid and dashed lines in the right panel express the fit results based on Eq. (19) at $m_{\rm PS}/m_{\rm V} = 0.65$ and 0.80, respectively.

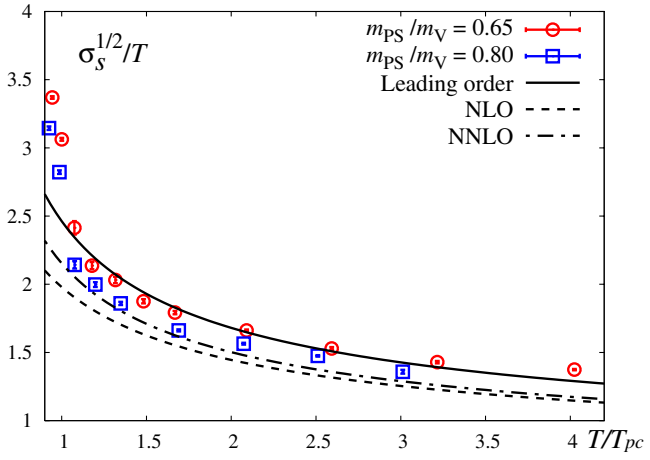

FIG. 17 (color online). Comparison of our results and predictions of the three-dimensional effective theory with contributions up to leading order (solid), NLO (dashed) and NNLO (dash-dotted line), respectively.

quite consistent with our lattice data. Similar agreement in quenched QCD has been reported in Ref. [21].

V. CONCLUSIONS

In the past few years, many of the lattice QCD simulations at finite temperature and density have been performed using staggered quark actions. However, to control the lattice artifacts, comparison with other quark actions are indispensable. This motivates us to carry out a systematic study with an improved Wilson quark action. As a first step, we performed simulations of $N_f = 2$ QCD on an $N_s^3 \times N_t = 16^3 \times 4$ lattice. We have identified the lines of constant physics and studied the temperature-dependence of various quantities at $m_{PS}/m_V = 0.65$ and 0.80 in the range $T/T_{pc} \sim 0.76$–4.0.

We found that, at $T \geq T_{pc}$, the free energies of QQ and $Q\bar{Q}$ normalized to be zero at large separation show attraction (repulsion) in the color-singlet and antitriplet channels (color octet and sextet channels). We fitted the free energy data in each channel by the screened Coulomb form, Eq. (11), which consists of the Casimir factor, the effective coupling $\alpha_{\rm eff}(T)$ and the Debye screening mass $m_D(T)$. We found that free energies in different channels can be fitted for $T \gtrsim 2T_{pc}$ in terms of universal $\alpha_{\rm eff}(T)$ and $m_D(T)$ while all the channel dependence can be absorbed by the Casimir factor. The magnitude and the T-dependence of $m_D(T)$ is consistent with the next-to-leading-order calculation in thermal perturbation theory. Moreover it is also well approximated by the leading-order form with an "effective" running coupling defined from $\alpha_{\rm eff}(T)$.

By comparing our results with the improved Wilson quark action and those with the improved staggered quark action, we found that $\alpha_{\rm eff}(T)$ does not show appreciable difference while $m_D(T)$ in the Wilson quark action is larger than that of the staggered quark action by 20%. To draw a definite conclusion, however, simulations with smaller lattice spacings, i.e., larger lattice sizes in the temporal direction (such as $N_t = 6$ or larger) at smaller quark masses are required.

We also discussed the force between heavy quarks to make a direct comparison of the free energies below and above T_{pc}. In the color octet channel, we find that the force becomes attractive below T_{pc} against the simple Casimir scaling law. This may be related to the suggestion that the Polyakov loop correlation in the octet channel is not independent from that in the singlet channel in the low temperature limit [36]. Moreover, spatial string tension $\sigma_s(T)$ in the high temperature phase was investigated. The result of the spatial string tension in the quark-gluon plasma shows a behavior consistent with $\sqrt{\sigma_s(T)} = c g_{2l}^2(2\pi T)T$ and agrees well with a parameter-free prediction of the NNLO three-dimensional effective theory.

Using our configurations, we are currently studying the critical temperature (T_{pc} in the chiral limit), the chiral and isospin susceptibility across the phase transition, the effect of the chemical potential on the heavy-quark free energies, and the equation of state at finite temperature and density. Some of the results are reported in Ref. [39,40].

ACKNOWLEDGMENTS

We would like to thank K.-I. Ishikawa and the members of the CP-PACS Collaboration for providing us with the basic code for generating the configurations. We also thank O. Kaczmarek for providing us the data from a staggered quark action. We are grateful to the Yukawa Institute for Theoretical Physics at Kyoto University for discussions during the YITP workshops YITP-W-06-07 and YKIS2006. This work is in part supported by Grants-in-Aid of the Japanese Ministry of Education, Culture, Sports, Science and Technology, (Nos. 13135204, 15540251, 17340066, 18540253, 18740134). S. E. is supported by the Sumitomo Foundation (No. 050408), and Y. M. is supported by the Japan Society for the Promotion of Science for Young Scientists. This work is in part supported also by the Large-Scale Numerical Simulation Projects of ACCC, Univ. of Tsukuba, and by the Large Scale Simulation Program of High Energy Accelerator Research Organization No. 06-19 (FY2006) of KEK.

APPENDIX A: FIT RANGE AND SYSTEMATIC ERRORS

In order to determine the appropriate fit range for free energies by the screened Coulomb form, Eq. (11), we estimate the effective Debye mass from the ratio of normalized free energies:

$$m_D^{\rm eff}(T;r) = \frac{1}{\Delta r}\log\frac{V_M(r)}{V_M(r+\Delta r)} - \frac{1}{\Delta r}\log\left[1+\frac{\Delta r}{r}\right]. \tag{A1}$$

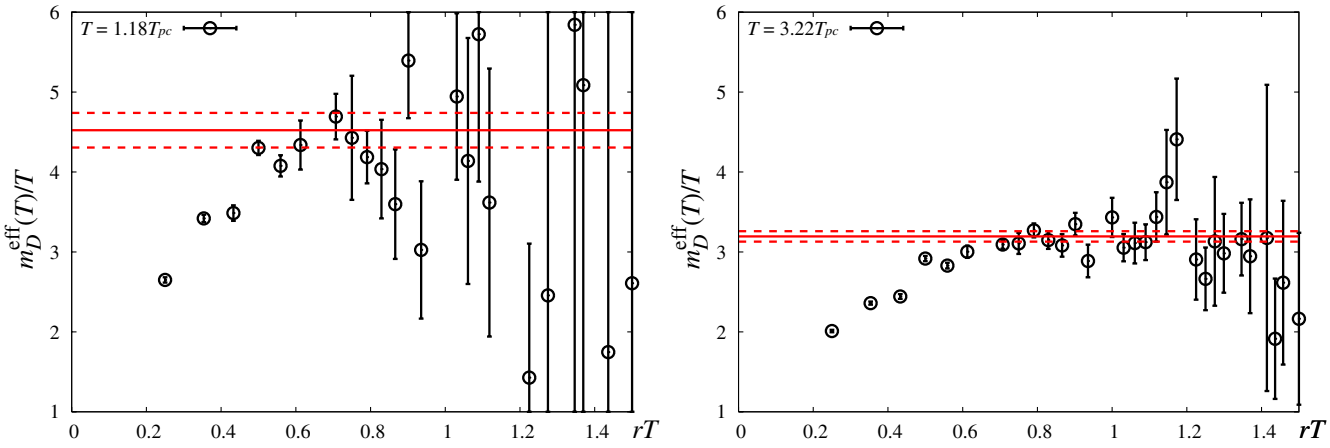

FIG. 18 (color online). The effective Debye mass defined by a ratio of normalized free energies, Eq. (A1), for color-singlet channel at $T = 1.18T_{\rm pc}$ (left) and $3.22T_{\rm pc}$ (right) for $m_{\rm PS}/m_{\rm V} = 0.65$. The fit results (statistical errors) are also given as solid lines (dashed lines).

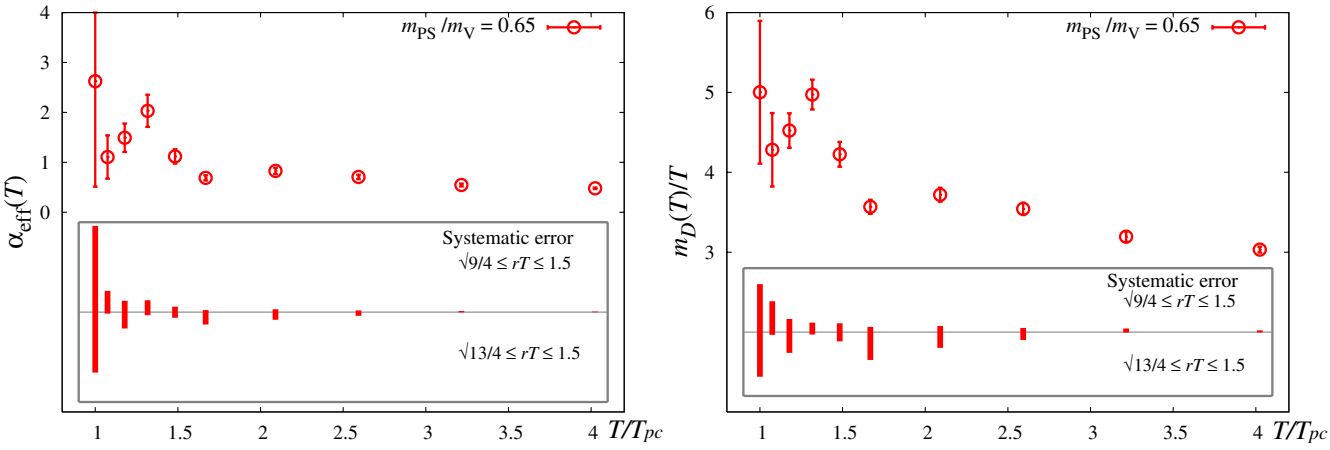

FIG. 19 (color online). The effective running coupling (left) and Debye screening mass (right) for color-singlet channel with the systematic errors due to the difference of the fit range defined in text at $m_{\rm PS}/m_{\rm V} = 0.65$.

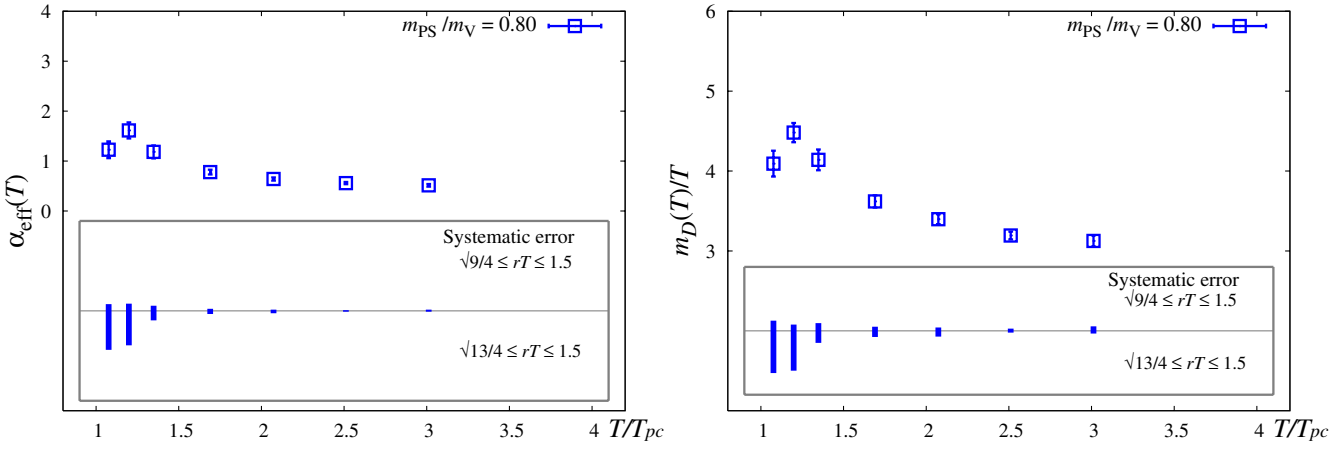

FIG. 20 (color online). The same figures with Fig. 19 at $m_{\rm PS}/m_{\rm V} = 0.80$.

The effective Debye mass is shown in Fig. 18 for color-singlet channel at $T = 1.18T_{pc}$ (left) and $3.22T_{pc}$ (right) for $m_{PS}/m_V = 0.65$. Since the plateaus of $m_D^{eff}(T;r)$ are found at $rT > 0.8$, we choose the fit range to be $\sqrt{11}/4 \le rT \le 1.5$. The solid lines in Fig. 18 are the results of the fit with the statistical errors indicated by the dashed lines.

In order to investigate systematic errors due to a dependence on fit ranges, we consider two other fit ranges: $\sqrt{9}/4 \le rT \le 1.5$ and $\sqrt{13}/4 \le rT \le 1.5$. The systematic errors due to the difference of the lower end of the fit range are shown in Fig. 19 for $\alpha_{eff}(T)$ (left) and $m_D(T)$ (right) in the color-singlet channel at $m_{PS}/m_V = 0.65$. The similar plots at $m_{PS}/m_V = 0.80$ are shown in Fig. 20. We find that, for $T \lesssim 2T_{pc}$, the systematic errors amount to at most the twice of the statistical errors, i.e. 2σ. On the other hand, for $T \gtrsim 2T_{pc}$, the systematic errors are less than 10% of the statistical errors.

APPENDIX B: DATA LISTS OF NORMALIZED FREE ENERGIES

In Tables V, VI, VII, VIII, IX, X, XI, XII, and XIII, we give data of the normalized free energies for all color channels and temperatures above T_{pc} as a function of distance (rT). The normalized free energies are measured at every ten trajectories for each quark mass and temperature summarized in Table I. The values in parenthesis of the normalized free energies express the statistical errors determined by a jackknife method with the bin-size of 100 trajectories.

TABLE V. Data lists of normalized free energies for all color channels at $T = 1.00T_{pc}$ (left) and $1.07T_{pc}$ (right) for $m_{PS}/m_V = 0.65$ as a function of rT.

	$T = 1.00T_{pc}$, $m_{PS}/m_V = 0.65$				$T = 1.07T_{pc}$, $m_{PS}/m_V = 0.65$			
rT	V_1	V_8	V_6	V_{3^*}	V_1	V_8	V_6	V_{3^*}
0.250	−2.3976(132)	−0.1786(59)	0.0466(78)	−1.0760(69)	−1.6513(71)	0.0337(27)	0.1796(31)	−0.7895(34)
0.354	−1.2753(110)	−0.1199(51)	−0.0228(56)	−0.5567(58)	−0.8627(51)	0.0041(18)	0.0783(24)	−0.4158(28)
0.433	−0.7376(104)	−0.0931(60)	−0.0390(75)	−0.3389(72)	−0.5205(46)	−0.0013(22)	0.0430(28)	−0.2525(27)
0.500	−0.5979(95)	−0.0956(74)	−0.0471(90)	−0.2766(90)	−0.4137(52)	−0.0085(25)	0.0251(26)	−0.2042(28)
0.559	−0.3640(72)	−0.0618(39)	−0.0352(42)	−0.1726(54)	−0.2728(33)	−0.0077(11)	0.0152(13)	−0.1388(19)
0.612	−0.2347(64)	−0.0503(38)	−0.0384(36)	−0.1287(54)	−0.1884(32)	−0.0087(13)	0.0076(15)	−0.0997(21)
0.707	−0.1170(118)	−0.0449(54)	−0.0405(56)	−0.0824(60)	−0.1117(39)	−0.0108(14)	0.0009(20)	−0.0638(21)
0.750	−0.1010(77)	−0.0318(42)	−0.0276(42)	−0.0577(51)	−0.0860(29)	−0.0091(11)	−0.0015(12)	−0.0507(16)
0.791	−0.0727(82)	−0.0241(34)	−0.0220(40)	−0.0425(50)	−0.0727(36)	−0.0073(15)	−0.0016(17)	−0.0418(18)
0.829	−0.0566(109)	−0.0223(35)	−0.0098(45)	−0.0405(53)	−0.0553(40)	−0.0072(12)	−0.0020(13)	−0.0324(17)
0.866	−0.0719(161)	−0.0232(55)	−0.0169(57)	−0.0485(101)	−0.0332(56)	−0.0037(22)	0.0006(25)	−0.0279(30)
0.901	−0.0364(97)	−0.0140(46)	−0.0170(41)	−0.0300(60)	−0.0361(29)	−0.0062(10)	−0.0028(12)	−0.0214(20)
0.935	−0.0401(72)	−0.0136(31)	−0.0171(33)	−0.0269(38)	−0.0295(26)	−0.0059(8)	−0.0033(11)	−0.0191(14)
1.000	−0.0045(212)	−0.0151(74)	−0.0007(92)	−0.0046(114)	−0.0234(54)	−0.0042(22)	−0.0008(23)	−0.0152(35)
1.031	−0.0157(64)	−0.0138(26)	−0.0115(32)	−0.0184(39)	−0.0147(24)	−0.0040(11)	−0.0016(11)	−0.0108(15)
1.061	−0.0203(71)	−0.0103(27)	−0.0093(32)	−0.0172(52)	−0.0177(28)	−0.0038(9)	−0.0038(12)	−0.0112(18)
1.090	−0.0305(92)	−0.0104(36)	−0.0053(40)	−0.0063(67)	−0.0082(38)	−0.0033(13)	−0.0027(13)	−0.0066(18)
1.118	0.0008(90)	−0.0158(35)	−0.0140(50)	−0.0206(58)	−0.0112(32)	−0.0048(11)	−0.0025(13)	−0.0051(17)
1.146	−0.0103(74)	−0.0073(25)	−0.0049(33)	−0.0097(38)	−0.0048(19)	−0.0032(10)	−0.0025(9)	−0.0057(14)
1.173	−0.0149(125)	−0.0109(45)	−0.0027(36)	−0.0027(64)	−0.0064(31)	−0.0034(13)	−0.0022(13)	−0.0072(18)
1.225	−0.0024(101)	−0.0056(31)	−0.0100(39)	−0.0127(49)	−0.0075(31)	−0.0029(11)	−0.0027(15)	−0.0066(18)
1.250	−0.0136(82)	−0.0068(33)	−0.0036(33)	−0.0127(57)	−0.0065(29)	−0.0028(11)	−0.0016(12)	−0.0045(17)
1.275	−0.0084(61)	−0.0047(18)	−0.0043(20)	−0.0080(33)	−0.0082(17)	−0.0018(8)	−0.0011(9)	−0.0044(12)
1.299	0.0162(83)	−0.0041(35)	−0.0043(35)	−0.0050(52)	−0.0045(24)	−0.0028(9)	−0.0022(11)	−0.0059(15)
1.346	−0.0008(63)	−0.0038(22)	−0.0010(23)	−0.0038(31)	−0.0043(19)	−0.0019(6)	−0.0011(7)	−0.0056(12)
1.369	−0.0070(79)	−0.0074(26)	−0.0075(31)	−0.0062(39)	−0.0038(19)	−0.0006(8)	−0.0013(9)	−0.0034(13)
1.414	−0.0106(159)	−0.0150(44)	0.0006(47)	−0.0137(88)	−0.0021(53)	−0.0015(13)	−0.0001(16)	−0.0037(26)
1.436	0.0013(73)	−0.0029(27)	−0.0006(34)	−0.0078(41)	−0.0042(22)	−0.0008(8)	−0.0005(10)	−0.0019(14)
1.458	−0.0112(70)	0.0013(28)	−0.0010(31)	−0.0095(47)	−0.0015(24)	−0.0003(10)	−0.0004(11)	−0.0014(15)
1.479	−0.0034(70)	−0.0036(29)	−0.0014(29)	0.0015(45)	−0.0012(22)	−0.0010(8)	−0.0010(9)	−0.0015(12)
1.500	0.0178(119)	0.0020(31)	0.0011(35)	−0.0078(62)	−0.0048(24)	−0.0013(9)	−0.0006(12)	−0.0031(16)

TABLE VI. Data lists of normalized free energies for all color channels at $T = 1.18T_{pc}$ (left) and $1.32T_{pc}$ (right) for $m_{PS}/m_V = 0.65$ as a function of rT.

	$T = 1.18T_{pc}$, $m_{PS}/m_V = 0.65$				$T = 1.32T_{pc}$, $m_{PS}/m_V = 0.65$			
rT	V_1	V_8	V_6	V_{3^*}	V_1	V_8	V_6	V_{3^*}
0.250	−1.3844(36)	0.0866(16)	0.2260(22)	−0.6711(18)	−1.2727(31)	0.1011(11)	0.2358(17)	−0.6208(17)
0.354	−0.7238(28)	0.0392(9)	0.1103(14)	−0.3518(15)	−0.6704(25)	0.0498(9)	0.1204(11)	−0.3280(16)
0.433	−0.4460(27)	0.0220(12)	0.0677(16)	−0.2183(17)	−0.4185(22)	0.0303(9)	0.0755(12)	−0.2075(15)
0.500	−0.3569(32)	0.0177(14)	0.0497(15)	−0.1749(20)	−0.3363(28)	0.0229(12)	0.0586(13)	−0.1649(16)
0.559	−0.2411(22)	0.0109(8)	0.0351(8)	−0.1196(13)	−0.2291(17)	0.0165(6)	0.0415(6)	−0.1128(10)
0.612	−0.1725(22)	0.0083(8)	0.0266(10)	−0.0861(12)	−0.1664(17)	0.0123(5)	0.0300(8)	−0.0825(11)
0.707	−0.1050(27)	0.0035(7)	0.0160(11)	−0.0541(16)	−0.1006(18)	0.0071(7)	0.0192(8)	−0.0495(12)
0.750	−0.0812(18)	0.0033(7)	0.0116(8)	−0.0418(10)	−0.0802(15)	0.0058(5)	0.0143(6)	−0.0393(9)
0.791	−0.0663(20)	0.0028(7)	0.0085(10)	−0.0350(10)	−0.0661(17)	0.0045(6)	0.0122(6)	−0.0334(8)
0.829	−0.0522(22)	0.0013(5)	0.0074(9)	−0.0271(11)	−0.0515(16)	0.0032(5)	0.0095(6)	−0.0273(9)
0.866	−0.0406(31)	0.0014(11)	0.0057(15)	−0.0228(18)	−0.0416(27)	0.0044(11)	0.0086(10)	−0.0194(17)
0.901	−0.0379(21)	0.0007(6)	0.0036(5)	−0.0199(12)	−0.0336(17)	0.0020(4)	0.0068(5)	−0.0166(8)
0.935	−0.0272(16)	0.0011(4)	0.0038(5)	−0.0148(9)	−0.0279(13)	0.0018(3)	0.0054(5)	−0.0135(7)
1.000	−0.0201(38)	−0.0004(12)	0.0024(12)	−0.0108(22)	−0.0201(26)	0.0034(9)	0.0042(10)	−0.0093(19)
1.031	−0.0186(15)	0.0007(4)	0.0028(6)	−0.0088(7)	−0.0160(11)	0.0016(4)	0.0034(5)	−0.0081(7)
1.061	−0.0141(19)	0.0003(5)	0.0024(7)	−0.0082(9)	−0.0131(13)	0.0013(4)	0.0031(4)	−0.0070(7)
1.090	−0.0139(22)	0.0001(6)	0.0008(7)	−0.0054(14)	−0.0106(17)	0.0007(4)	0.0018(5)	−0.0057(9)
1.118	−0.0127(19)	−0.0006(6)	0.0007(7)	−0.0057(10)	−0.0095(16)	0.0011(6)	0.0026(6)	−0.0035(8)
1.146	−0.0080(13)	0.0009(5)	0.0012(6)	−0.0049(7)	−0.0081(11)	0.0009(3)	0.0019(5)	−0.0038(6)
1.173	−0.0106(21)	−0.0002(7)	0.0012(7)	−0.0070(11)	−0.0056(18)	0.0014(4)	0.0012(6)	−0.0021(10)
1.225	−0.0063(19)	−0.0006(6)	0.0000(7)	−0.0034(11)	−0.0051(17)	0.0006(5)	0.0017(7)	−0.0023(7)
1.250	−0.0036(18)	−0.0003(7)	0.0005(7)	−0.0023(10)	−0.0058(11)	−0.0002(4)	0.0004(4)	−0.0026(6)
1.275	−0.0045(12)	−0.0003(4)	0.0010(5)	−0.0026(7)	−0.0036(9)	−0.0001(2)	0.0005(4)	−0.0019(6)
1.299	−0.0043(15)	−0.0002(5)	−0.0001(6)	−0.0013(9)	−0.0027(15)	−0.0003(4)	0.0002(4)	−0.0016(7)
1.346	−0.0026(11)	0.0003(4)	0.0004(4)	−0.0017(6)	−0.0016(8)	0.0006(3)	0.0007(3)	−0.0009(5)
1.369	−0.0042(16)	−0.0002(4)	−0.0003(5)	−0.0028(8)	−0.0028(12)	0.0002(3)	0.0001(3)	−0.0010(7)
1.414	−0.0002(25)	0.0002(9)	0.0006(11)	0.0009(16)	−0.0069(24)	0.0001(7)	0.0003(7)	−0.0008(11)
1.436	−0.0006(15)	0.0001(5)	0.0000(5)	−0.0008(7)	0.0007(12)	−0.0005(3)	−0.0003(4)	0.0002(6)
1.458	−0.0016(15)	0.0004(4)	0.0004(5)	0.0004(9)	−0.0015(10)	0.0008(4)	0.0006(4)	−0.0010(5)
1.479	−0.0037(12)	−0.0003(5)	−0.0007(5)	−0.0008(6)	−0.0011(11)	0.0006(4)	0.0006(4)	−0.0006(5)
1.500	−0.0040(19)	−0.0009(6)	−0.0012(7)	0.0001(9)	0.0005(12)	0.0004(3)	0.0009(4)	0.0001(8)

TABLE VII. Data lists of normalized free energies for all color channels at $T = 1.48T_{pc}$ (left) and $1.67T_{pc}$ (right) for $m_{PS}/m_V = 0.65$ as a function of rT.

	$T = 1.48T_{pc}$, $m_{PS}/m_V = 0.65$				$T = 1.67T_{pc}$, $m_{PS}/m_V = 0.65$			
rT	$V_{\mathbf{1}}$	$V_{\mathbf{8}}$	$V_{\mathbf{6}}$	$V_{\mathbf{3^*}}$	$V_{\mathbf{1}}$	$V_{\mathbf{8}}$	$V_{\mathbf{6}}$	$V_{\mathbf{3^*}}$
0.250	−1.1929(27)	0.1064(12)	0.2382(16)	−0.5850(14)	−1.1278(24)	0.1107(9)	0.2366(12)	−0.5522(12)
0.354	−0.6369(22)	0.0549(7)	0.1237(10)	−0.3118(12)	−0.6082(22)	0.0580(6)	0.1257(7)	−0.2983(11)
0.433	−0.4032(25)	0.0350(7)	0.0781(9)	−0.1979(12)	−0.3905(20)	0.0374(6)	0.0813(10)	−0.1925(11)
0.500	−0.3218(24)	0.0277(8)	0.0643(9)	−0.1595(15)	−0.3144(22)	0.0288(6)	0.0643(8)	−0.1554(13)
0.559	−0.2268(19)	0.0192(4)	0.0437(6)	−0.1110(10)	−0.2227(17)	0.0214(4)	0.0471(5)	−0.1105(9)
0.612	−0.1644(17)	0.0144(5)	0.0318(7)	−0.0817(9)	−0.1665(14)	0.0162(4)	0.0348(5)	−0.0828(8)
0.707	−0.1042(18)	0.0108(5)	0.0220(8)	−0.0511(9)	−0.1051(16)	0.0103(5)	0.0225(6)	−0.0531(9)
0.750	−0.0818(15)	0.0074(4)	0.0167(6)	−0.0407(7)	−0.0849(13)	0.0082(3)	0.0179(4)	−0.0430(7)
0.791	−0.0697(15)	0.0066(4)	0.0142(5)	−0.0340(9)	−0.0700(13)	0.0072(4)	0.0151(5)	−0.0348(7)
0.829	−0.0534(14)	0.0054(4)	0.0113(4)	−0.0284(7)	−0.0586(13)	0.0059(4)	0.0131(4)	−0.0295(6)
0.866	−0.0437(22)	0.0053(6)	0.0098(9)	−0.0213(16)	−0.0419(18)	0.0040(6)	0.0089(6)	−0.0228(9)
0.901	−0.0380(13)	0.0039(4)	0.0077(5)	−0.0189(6)	−0.0414(12)	0.0041(3)	0.0091(5)	−0.0204(6)
0.935	−0.0317(11)	0.0028(2)	0.0064(4)	−0.0158(6)	−0.0342(11)	0.0031(2)	0.0071(3)	−0.0173(5)
1.000	−0.0185(28)	0.0019(8)	0.0048(10)	−0.0097(13)	−0.0249(21)	0.0019(7)	0.0046(8)	−0.0124(12)
1.031	−0.0183(10)	0.0020(3)	0.0042(4)	−0.0087(5)	−0.0216(9)	0.0020(2)	0.0044(3)	−0.0114(5)
1.061	−0.0168(11)	0.0012(3)	0.0038(4)	−0.0086(5)	−0.0195(7)	0.0022(2)	0.0043(3)	−0.0096(5)
1.090	−0.0164(14)	0.0019(3)	0.0033(4)	−0.0065(7)	−0.0157(12)	0.0014(3)	0.0033(5)	−0.0083(7)
1.118	−0.0128(15)	0.0015(4)	0.0028(4)	−0.0069(8)	−0.0138(11)	0.0021(3)	0.0035(4)	−0.0063(6)
1.146	−0.0113(11)	0.0011(3)	0.0023(3)	−0.0056(6)	−0.0127(8)	0.0014(3)	0.0028(3)	−0.0059(4)
1.173	−0.0103(14)	0.0016(4)	0.0020(5)	−0.0042(7)	−0.0097(10)	0.0007(3)	0.0029(4)	−0.0067(7)
1.225	−0.0062(12)	0.0012(5)	0.0021(5)	−0.0033(8)	−0.0086(12)	0.0006(3)	0.0013(3)	−0.0048(6)
1.250	−0.0050(11)	0.0008(3)	0.0022(4)	−0.0031(6)	−0.0076(9)	0.0015(2)	0.0021(3)	−0.0035(5)
1.275	−0.0055(9)	0.0004(2)	0.0015(2)	−0.0032(5)	−0.0068(8)	0.0007(2)	0.0017(3)	−0.0037(4)
1.299	−0.0053(12)	0.0005(4)	0.0008(4)	−0.0025(7)	−0.0066(8)	0.0006(3)	0.0013(3)	−0.0033(5)
1.346	−0.0056(8)	0.0007(2)	0.0013(3)	−0.0022(5)	−0.0050(8)	0.0005(2)	0.0013(2)	−0.0028(4)
1.369	−0.0039(11)	0.0006(3)	0.0010(4)	−0.0024(5)	−0.0040(10)	0.0004(2)	0.0012(3)	−0.0024(5)
1.414	−0.0021(18)	0.0012(5)	0.0014(6)	−0.0013(10)	−0.0010(14)	0.0003(5)	0.0009(5)	−0.0024(8)
1.436	−0.0036(8)	0.0006(2)	0.0010(3)	−0.0019(5)	−0.0030(9)	0.0003(2)	0.0005(3)	−0.0016(5)
1.458	−0.0023(9)	0.0003(2)	0.0009(4)	−0.0009(5)	−0.0032(7)	0.0004(2)	0.0009(2)	−0.0013(5)
1.479	−0.0031(8)	0.0003(2)	0.0008(3)	−0.0016(4)	−0.0021(8)	−0.0001(2)	0.0004(3)	−0.0008(4)
1.500	−0.0039(11)	0.0002(3)	0.0009(4)	−0.0012(7)	−0.0005(10)	0.0003(2)	0.0007(3)	−0.0007(6)

TABLE VIII. Data lists of normalized free energies for all color channels at $T = 2.09T_{pc}$ (left) and $2.59T_{pc}$ (right) for $m_{PS}/m_V = 0.65$ as a function of rT.

	$T = 2.09T_{pc}$, $m_{PS}/m_V = 0.65$				$T = 2.59T_{pc}$, $m_{PS}/m_V = 0.65$			
rT	V_1	V_8	V_6	V_{3^*}	V_1	V_8	V_6	V_{3^*}
0.250	−1.0261(19)	0.1090(6)	0.2275(10)	−0.5062(10)	−0.9461(18)	0.1062(4)	0.2181(7)	−0.4681(9)
0.354	−0.5610(16)	0.0585(4)	0.1228(6)	−0.2767(8)	−0.5241(15)	0.0574(3)	0.1190(5)	−0.2592(8)
0.433	−0.3661(16)	0.0386(4)	0.0803(6)	−0.1808(8)	−0.3467(13)	0.0381(3)	0.0789(5)	−0.1724(7)
0.500	−0.2964(15)	0.0302(5)	0.0634(7)	−0.1457(8)	−0.2781(16)	0.0309(4)	0.0634(5)	−0.1370(8)
0.559	−0.2132(12)	0.0218(3)	0.0468(4)	−0.1055(6)	−0.2044(11)	0.0223(2)	0.0466(4)	−0.1013(6)
0.612	−0.1607(12)	0.0166(3)	0.0349(3)	−0.0801(6)	−0.1562(11)	0.0171(2)	0.0356(3)	−0.0771(5)
0.707	−0.1044(14)	0.0116(4)	0.0238(5)	−0.0518(6)	−0.1035(11)	0.0115(2)	0.0237(3)	−0.0513(6)
0.750	−0.0855(10)	0.0092(2)	0.0187(3)	−0.0425(5)	−0.0840(9)	0.0097(2)	0.0196(2)	−0.0414(4)
0.791	−0.0726(9)	0.0077(2)	0.0161(3)	−0.0363(5)	−0.0711(9)	0.0081(2)	0.0163(2)	−0.0350(5)
0.829	−0.0593(9)	0.0060(2)	0.0131(3)	−0.0291(5)	−0.0598(9)	0.0069(1)	0.0138(2)	−0.0291(5)
0.866	−0.0489(14)	0.0064(4)	0.0118(5)	−0.0232(8)	−0.0502(13)	0.0058(3)	0.0114(4)	−0.0245(6)
0.901	−0.0428(9)	0.0052(3)	0.0105(4)	−0.0212(4)	−0.0427(9)	0.0048(2)	0.0102(2)	−0.0215(4)
0.935	−0.0365(7)	0.0039(1)	0.0083(2)	−0.0180(4)	−0.0361(8)	0.0040(1)	0.0085(2)	−0.0181(4)
1.000	−0.0235(16)	0.0032(5)	0.0060(5)	−0.0126(9)	−0.0279(11)	0.0030(4)	0.0069(5)	−0.0144(7)
1.031	−0.0235(8)	0.0025(1)	0.0056(2)	−0.0118(4)	−0.0236(7)	0.0028(1)	0.0054(2)	−0.0118(4)
1.061	−0.0197(8)	0.0020(2)	0.0047(3)	−0.0100(4)	−0.0206(6)	0.0023(1)	0.0050(2)	−0.0104(3)
1.090	−0.0181(10)	0.0019(3)	0.0042(3)	−0.0085(4)	−0.0178(8)	0.0023(2)	0.0045(2)	−0.0094(3)
1.118	−0.0162(9)	0.0019(2)	0.0037(3)	−0.0075(4)	−0.0156(7)	0.0020(2)	0.0039(2)	−0.0079(4)
1.146	−0.0134(7)	0.0016(1)	0.0033(2)	−0.0067(4)	−0.0133(6)	0.0017(1)	0.0033(1)	−0.0067(2)
1.173	−0.0130(10)	0.0014(2)	0.0029(3)	−0.0065(4)	−0.0119(8)	0.0015(2)	0.0026(3)	−0.0058(4)
1.225	−0.0093(9)	0.0008(2)	0.0017(3)	−0.0048(5)	−0.0090(8)	0.0012(2)	0.0024(2)	−0.0041(3)
1.250	−0.0080(9)	0.0013(2)	0.0021(3)	−0.0036(5)	−0.0079(7)	0.0011(1)	0.0023(2)	−0.0039(4)
1.275	−0.0076(6)	0.0008(1)	0.0018(2)	−0.0036(3)	−0.0076(5)	0.0012(1)	0.0021(1)	−0.0039(2)
1.299	−0.0069(6)	0.0005(2)	0.0015(2)	−0.0037(3)	−0.0069(6)	0.0011(1)	0.0019(2)	−0.0036(3)
1.346	−0.0058(6)	0.0009(2)	0.0015(2)	−0.0029(3)	−0.0060(5)	0.0007(1)	0.0013(1)	−0.0029(2)
1.369	−0.0035(5)	0.0004(1)	0.0009(1)	−0.0019(3)	−0.0052(5)	0.0006(1)	0.0012(1)	−0.0025(2)
1.414	−0.0036(11)	0.0009(3)	0.0014(4)	−0.0013(7)	−0.0046(10)	0.0006(2)	0.0010(3)	−0.0020(5)
1.436	−0.0020(6)	0.0003(1)	0.0006(2)	−0.0013(4)	−0.0034(6)	0.0004(1)	0.0006(1)	−0.0014(3)
1.458	−0.0035(7)	0.0002(2)	0.0007(2)	−0.0021(4)	−0.0030(7)	0.0003(1)	0.0004(1)	−0.0015(3)
1.479	−0.0029(7)	0.0001(1)	0.0006(2)	−0.0015(3)	−0.0024(5)	0.0004(1)	0.0008(2)	−0.0010(2)
1.500	−0.0025(8)	0.0002(2)	0.0006(3)	−0.0012(4)	−0.0020(7)	0.0005(1)	0.0007(2)	−0.0013(3)

TABLE IX. Data lists of normalized free energies for all color channels at $T = 3.22T_{pc}$ (left) and $4.02T_{pc}$ (right) for $m_{PS}/m_V = 0.65$ as a function of rT.

	$T = 3.22T_{pc}$, $m_{PS}/m_V = 0.65$				$T = 4.02T_{pc}$, $m_{PS}/m_V = 0.65$			
rT	$V_{\mathbf{1}}$	$V_{\mathbf{8}}$	$V_{\mathbf{6}}$	$V_{\mathbf{3^*}}$	$V_{\mathbf{1}}$	$V_{\mathbf{8}}$	$V_{\mathbf{6}}$	$V_{\mathbf{3^*}}$
0.250	−0.8865(16)	0.1026(5)	0.2090(7)	−0.4398(8)	−0.8365(16)	0.0986(4)	0.1994(6)	−0.4159(8)
0.354	−0.4962(15)	0.0566(3)	0.1158(5)	−0.2461(8)	−0.4731(15)	0.0547(3)	0.1116(4)	−0.2352(7)
0.433	−0.3332(15)	0.0380(3)	0.0773(4)	−0.1649(8)	−0.3194(15)	0.0362(2)	0.0749(4)	−0.1591(7)
0.500	−0.2681(12)	0.0303(2)	0.0622(4)	−0.1329(7)	−0.2579(12)	0.0294(3)	0.0602(4)	−0.1280(6)
0.559	−0.2000(10)	0.0225(2)	0.0463(3)	−0.0993(5)	−0.1937(10)	0.0224(1)	0.0454(3)	−0.0961(5)
0.612	−0.1556(11)	0.0175(2)	0.0360(2)	−0.0772(5)	−0.1518(10)	0.0172(2)	0.0353(3)	−0.0752(5)
0.707	−0.1045(10)	0.0119(2)	0.0243(3)	−0.0517(6)	−0.1030(9)	0.0118(2)	0.0241(2)	−0.0511(5)
0.750	−0.0862(8)	0.0098(1)	0.0201(2)	−0.0430(4)	−0.0850(7)	0.0095(1)	0.0197(2)	−0.0424(4)
0.791	−0.0735(9)	0.0083(2)	0.0172(2)	−0.0367(4)	−0.0726(9)	0.0083(2)	0.0169(2)	−0.0361(4)
0.829	−0.0615(8)	0.0071(1)	0.0145(2)	−0.0308(4)	−0.0617(7)	0.0069(1)	0.0145(2)	−0.0308(3)
0.866	−0.0514(11)	0.0065(3)	0.0125(4)	−0.0250(6)	−0.0522(7)	0.0061(2)	0.0127(3)	−0.0263(5)
0.901	−0.0450(7)	0.0051(2)	0.0105(3)	−0.0225(4)	−0.0456(7)	0.0053(1)	0.0109(1)	−0.0228(3)
0.935	−0.0390(7)	0.0046(1)	0.0093(2)	−0.0195(4)	−0.0392(5)	0.0045(1)	0.0093(1)	−0.0197(3)
1.000	−0.0297(10)	0.0036(2)	0.0069(3)	−0.0148(5)	−0.0288(12)	0.0029(2)	0.0065(3)	−0.0146(6)
1.031	−0.0257(6)	0.0031(1)	0.0060(1)	−0.0129(3)	−0.0266(5)	0.0030(1)	0.0063(1)	−0.0132(2)
1.061	−0.0229(6)	0.0025(1)	0.0053(2)	−0.0116(3)	−0.0239(5)	0.0028(1)	0.0057(1)	−0.0120(3)
1.090	−0.0206(6)	0.0027(1)	0.0054(2)	−0.0105(3)	−0.0214(6)	0.0024(1)	0.0048(1)	−0.0103(3)
1.118	−0.0183(7)	0.0019(1)	0.0042(2)	−0.0093(4)	−0.0185(6)	0.0020(1)	0.0043(2)	−0.0092(3)
1.146	−0.0156(6)	0.0018(1)	0.0037(1)	−0.0079(3)	−0.0165(5)	0.0019(1)	0.0040(1)	−0.0083(2)
1.173	−0.0157(8)	0.0019(1)	0.0035(1)	−0.0077(4)	−0.0133(6)	0.0020(1)	0.0037(1)	−0.0066(2)
1.225	−0.0107(7)	0.0011(1)	0.0024(2)	−0.0053(4)	−0.0112(5)	0.0013(1)	0.0027(2)	−0.0056(3)
1.250	−0.0101(6)	0.0011(1)	0.0026(1)	−0.0055(3)	−0.0108(5)	0.0013(1)	0.0027(1)	−0.0054(2)
1.275	−0.0099(5)	0.0012(0)	0.0025(1)	−0.0050(2)	−0.0100(4)	0.0012(0)	0.0024(1)	−0.0051(2)
1.299	−0.0089(6)	0.0011(1)	0.0022(1)	−0.0044(3)	−0.0088(4)	0.0012(1)	0.0021(1)	−0.0044(2)
1.346	−0.0075(4)	0.0009(1)	0.0018(1)	−0.0037(2)	−0.0069(4)	0.0009(0)	0.0019(1)	−0.0035(2)
1.369	−0.0063(5)	0.0007(1)	0.0017(1)	−0.0034(3)	−0.0068(5)	0.0008(1)	0.0017(1)	−0.0033(2)
1.414	−0.0045(8)	0.0007(2)	0.0015(2)	−0.0023(4)	−0.0052(8)	0.0006(1)	0.0012(2)	−0.0031(5)
1.436	−0.0047(5)	0.0006(1)	0.0012(1)	−0.0023(2)	−0.0043(4)	0.0006(1)	0.0011(1)	−0.0022(2)
1.458	−0.0046(5)	0.0005(1)	0.0012(1)	−0.0023(2)	−0.0044(4)	0.0005(0)	0.0010(1)	−0.0022(2)
1.479	−0.0042(6)	0.0006(1)	0.0010(1)	−0.0020(3)	−0.0047(4)	0.0006(1)	0.0011(1)	−0.0022(2)
1.500	−0.0043(5)	0.0003(1)	0.0008(1)	−0.0024(3)	−0.0030(5)	0.0005(1)	0.0009(1)	−0.0015(3)

TABLE X. Data lists of normalized free energies for all color channels at $T = 1.08T_{pc}$ (left) and $1.20T_{pc}$ (right) for $m_{PS}/m_V = 0.80$ as a function of rT.

	$T = 1.08T_{pc}$, $m_{PS}/m_V = 0.80$				$T = 1.20T_{pc}$, $m_{PS}/m_V = 0.80$			
rT	V_1	V_8	V_6	V_{3^*}	V_1	V_8	V_6	V_{3^*}
0.250	−1.5314(50)	0.0740(18)	0.2251(23)	−0.7414(28)	−1.3096(35)	0.1048(12)	0.2435(15)	−0.6396(18)
0.354	−0.8417(43)	0.0276(14)	0.1075(16)	−0.4103(25)	−0.7118(31)	0.0524(9)	0.1263(10)	−0.3491(15)
0.433	−0.5350(35)	0.0112(14)	0.0618(15)	−0.2644(23)	−0.4546(25)	0.0322(8)	0.0795(10)	−0.2238(13)
0.500	−0.4250(36)	0.0081(14)	0.0469(18)	−0.2128(19)	−0.3705(25)	0.0250(10)	0.0644(13)	−0.1813(16)
0.559	−0.2980(26)	0.0042(9)	0.0298(10)	−0.1484(17)	−0.2579(20)	0.0170(7)	0.0436(7)	−0.1277(11)
0.612	−0.2145(24)	0.0001(8)	0.0199(9)	−0.1087(15)	−0.1898(18)	0.0124(5)	0.0317(6)	−0.0950(10)
0.707	−0.1330(29)	−0.0005(12)	0.0112(15)	−0.0648(16)	−0.1152(18)	0.0078(6)	0.0188(6)	−0.0573(9)
0.750	−0.1048(23)	−0.0022(8)	0.0067(10)	−0.0541(13)	−0.0949(15)	0.0053(3)	0.0156(5)	−0.0482(8)
0.791	−0.0855(21)	−0.0021(7)	0.0063(9)	−0.0435(11)	−0.0787(16)	0.0050(5)	0.0136(5)	−0.0407(9)
0.829	−0.0673(21)	−0.0025(8)	0.0033(9)	−0.0348(11)	−0.0639(15)	0.0035(4)	0.0107(4)	−0.0332(8)
0.866	−0.0507(32)	−0.0039(12)	0.0028(14)	−0.0281(18)	−0.0468(25)	0.0025(8)	0.0085(10)	−0.0246(12)
0.901	−0.0463(22)	−0.0018(8)	0.0019(9)	−0.0239(14)	−0.0421(14)	0.0026(4)	0.0077(5)	−0.0221(8)
0.935	−0.0408(19)	−0.0019(7)	0.0014(7)	−0.0209(9)	−0.0340(10)	0.0017(3)	0.0056(4)	−0.0182(7)
1.000	−0.0323(40)	−0.0027(14)	−0.0004(16)	−0.0165(22)	−0.0275(25)	0.0025(8)	0.0048(10)	−0.0136(15)
1.031	−0.0251(16)	−0.0016(5)	0.0000(6)	−0.0118(8)	−0.0211(11)	0.0014(4)	0.0036(5)	−0.0109(6)
1.061	−0.0185(16)	−0.0020(6)	0.0000(7)	−0.0108(9)	−0.0178(11)	0.0008(4)	0.0036(5)	−0.0097(6)
1.090	−0.0149(21)	−0.0012(8)	−0.0001(9)	−0.0102(11)	−0.0177(14)	0.0003(4)	0.0019(6)	−0.0079(7)
1.118	−0.0157(21)	−0.0024(7)	0.0003(8)	−0.0097(12)	−0.0140(13)	0.0001(4)	0.0016(5)	−0.0072(7)
1.146	−0.0137(16)	−0.0019(6)	−0.0005(6)	−0.0070(8)	−0.0109(11)	0.0006(3)	0.0017(4)	−0.0060(6)
1.173	−0.0118(23)	−0.0021(6)	−0.0017(9)	−0.0058(13)	−0.0095(15)	0.0001(5)	0.0013(7)	−0.0043(9)
1.225	−0.0078(18)	−0.0013(6)	−0.0006(6)	−0.0054(11)	−0.0055(15)	0.0005(3)	0.0014(5)	−0.0028(7)
1.250	−0.0072(18)	−0.0019(6)	−0.0023(7)	−0.0045(9)	−0.0076(12)	−0.0004(4)	0.0009(4)	−0.0046(6)
1.275	−0.0061(13)	−0.0011(5)	−0.0008(5)	−0.0036(8)	−0.0061(8)	0.0003(3)	0.0013(3)	−0.0031(5)
1.299	−0.0058(16)	−0.0018(6)	−0.0015(7)	−0.0035(9)	−0.0078(11)	0.0000(4)	0.0010(5)	−0.0033(7)
1.346	−0.0049(11)	−0.0006(5)	−0.0001(5)	−0.0027(7)	−0.0026(9)	−0.0001(3)	0.0007(3)	−0.0016(5)
1.369	−0.0048(13)	−0.0012(5)	−0.0006(6)	−0.0031(9)	−0.0028(11)	−0.0002(2)	0.0002(3)	−0.0020(6)
1.414	−0.0019(26)	−0.0021(8)	−0.0021(10)	−0.0022(19)	−0.0016(22)	−0.0009(5)	−0.0004(7)	−0.0023(11)
1.436	−0.0031(14)	−0.0012(6)	−0.0004(7)	−0.0013(7)	−0.0011(9)	−0.0003(3)	−0.0006(4)	−0.0011(5)
1.458	−0.0031(13)	−0.0012(5)	−0.0007(6)	−0.0018(8)	−0.0019(10)	0.0006(4)	0.0007(4)	−0.0011(5)
1.479	−0.0024(14)	−0.0007(5)	−0.0008(5)	−0.0012(8)	−0.0023(10)	0.0000(3)	0.0003(4)	−0.0011(6)
1.500	0.0007(21)	−0.0012(7)	−0.0013(8)	−0.0013(11)	−0.0005(13)	−0.0004(3)	−0.0006(5)	−0.0007(7)

TABLE XI. Data lists of normalized free energies for all color channels at $T = 1.35T_{pc}$ (left) and $1.69T_{pc}$ (right) for $m_{PS}/m_V = 0.80$ as a function of rT.

	$T = 1.35T_{pc}$, $m_{PS}/m_V = 0.80$				$T = 1.69T_{pc}$, $m_{PS}/m_V = 0.80$			
rT	$V_{\mathbf{1}}$	$V_{\mathbf{8}}$	$V_{\mathbf{6}}$	$V_{\mathbf{3}^*}$	$V_{\mathbf{1}}$	$V_{\mathbf{8}}$	$V_{\mathbf{6}}$	$V_{\mathbf{3}^*}$
0.250	−1.1850(27)	0.1111(11)	0.2410(14)	−0.5807(14)	−1.0540(23)	0.1117(7)	0.2324(11)	−0.5205(13)
0.354	−0.6453(21)	0.0573(7)	0.1282(10)	−0.3159(11)	−0.5794(20)	0.0602(5)	0.1268(7)	−0.2858(10)
0.433	−0.4158(22)	0.0378(8)	0.0830(10)	−0.2033(10)	−0.3787(19)	0.0389(5)	0.0824(7)	−0.1869(11)
0.500	−0.3392(22)	0.0299(7)	0.0660(7)	−0.1657(12)	−0.3048(18)	0.0312(5)	0.0661(6)	−0.1504(9)
0.559	−0.2379(15)	0.0209(5)	0.0471(6)	−0.1172(7)	−0.2213(17)	0.0226(3)	0.0481(4)	−0.1095(8)
0.612	−0.1767(15)	0.0160(4)	0.0361(5)	−0.0873(8)	−0.1674(14)	0.0172(3)	0.0365(4)	−0.0827(7)
0.707	−0.1108(15)	0.0096(5)	0.0233(6)	−0.0548(8)	−0.1078(15)	0.0111(3)	0.0238(4)	−0.0537(8)
0.750	−0.0887(11)	0.0084(3)	0.0183(3)	−0.0441(5)	−0.0880(13)	0.0093(2)	0.0199(3)	−0.0437(6)
0.791	−0.0768(16)	0.0075(4)	0.0164(6)	−0.0374(7)	−0.0737(13)	0.0075(3)	0.0166(4)	−0.0367(6)
0.829	−0.0617(13)	0.0056(3)	0.0131(4)	−0.0309(6)	−0.0626(13)	0.0064(3)	0.0132(4)	−0.0304(5)
0.866	−0.0475(20)	0.0047(6)	0.0106(7)	−0.0243(11)	−0.0514(15)	0.0058(4)	0.0114(5)	−0.0258(8)
0.901	−0.0423(13)	0.0038(3)	0.0081(4)	−0.0210(8)	−0.0448(11)	0.0047(2)	0.0098(4)	−0.0219(6)
0.935	−0.0357(10)	0.0031(2)	0.0073(3)	−0.0183(5)	−0.0373(10)	0.0041(1)	0.0084(2)	−0.0184(5)
1.000	−0.0287(25)	0.0034(7)	0.0068(9)	−0.0126(13)	−0.0309(20)	0.0030(5)	0.0059(6)	−0.0149(10)
1.031	−0.0222(9)	0.0021(2)	0.0046(3)	−0.0111(5)	−0.0244(7)	0.0024(2)	0.0052(2)	−0.0117(4)
1.061	−0.0194(12)	0.0022(2)	0.0039(4)	−0.0095(6)	−0.0213(9)	0.0023(2)	0.0052(2)	−0.0105(5)
1.090	−0.0173(12)	0.0016(3)	0.0037(5)	−0.0088(7)	−0.0181(10)	0.0019(2)	0.0039(3)	−0.0095(5)
1.118	−0.0144(10)	0.0018(3)	0.0028(3)	−0.0066(6)	−0.0163(11)	0.0019(2)	0.0038(3)	−0.0084(6)
1.146	−0.0129(8)	0.0010(2)	0.0027(3)	−0.0063(5)	−0.0149(8)	0.0017(2)	0.0033(2)	−0.0068(4)
1.173	−0.0093(12)	0.0007(3)	0.0017(4)	−0.0054(6)	−0.0128(10)	0.0018(2)	0.0032(3)	−0.0057(5)
1.225	−0.0084(11)	0.0011(3)	0.0017(4)	−0.0038(6)	−0.0100(9)	0.0005(2)	0.0021(3)	−0.0044(5)
1.250	−0.0092(12)	0.0010(3)	0.0012(3)	−0.0038(6)	−0.0085(9)	0.0007(2)	0.0020(2)	−0.0045(4)
1.275	−0.0064(8)	0.0006(2)	0.0014(3)	−0.0036(5)	−0.0072(6)	0.0007(2)	0.0016(2)	−0.0037(3)
1.299	−0.0060(10)	0.0004(2)	0.0017(3)	−0.0032(5)	−0.0077(9)	0.0005(2)	0.0012(3)	−0.0036(4)
1.346	−0.0040(8)	0.0005(2)	0.0007(2)	−0.0019(4)	−0.0052(6)	0.0008(2)	0.0015(2)	−0.0024(3)
1.369	−0.0045(9)	0.0004(2)	0.0006(3)	−0.0022(6)	−0.0053(8)	0.0006(2)	0.0008(3)	−0.0022(4)
1.414	−0.0045(16)	−0.0002(4)	−0.0002(5)	−0.0024(11)	−0.0043(11)	0.0004(3)	0.0011(4)	−0.0016(8)
1.436	−0.0030(7)	−0.0001(2)	0.0004(3)	−0.0021(5)	−0.0037(8)	−0.0001(2)	0.0006(2)	−0.0020(3)
1.458	−0.0033(9)	0.0004(2)	0.0008(3)	−0.0019(5)	−0.0043(7)	0.0002(2)	0.0008(2)	−0.0021(3)
1.479	−0.0030(9)	0.0003(3)	0.0009(3)	−0.0015(5)	−0.0033(6)	0.0001(2)	0.0005(2)	−0.0019(3)
1.500	−0.0042(10)	0.0003(3)	0.0006(3)	−0.0012(5)	−0.0021(8)	0.0003(2)	0.0006(3)	−0.0013(4)

TABLE XII. Data lists of normalized free energies for all color channels at $T = 2.07T_{pc}$ (left) and $2.51T_{pc}$ (right) for $m_{PS}/m_V = 0.80$ as a function of rT.

	$T = 2.07T_{pc}$, $m_{PS}/m_V = 0.80$				$T = 2.51T_{pc}$, $m_{PS}/m_V = 0.80$			
rT	V_1	V_8	V_6	V_{3^*}	V_1	V_8	V_6	V_{3^*}
0.250	−0.9651(22)	0.1079(6)	0.2230(9)	−0.4778(11)	−0.8995(18)	0.1029(4)	0.2105(6)	−0.4463(9)
0.354	−0.5365(19)	0.0589(4)	0.1218(6)	−0.2650(9)	−0.5053(16)	0.0571(3)	0.1173(5)	−0.2503(8)
0.433	−0.3561(19)	0.0387(5)	0.0814(6)	−0.1766(9)	−0.3385(14)	0.0384(3)	0.0787(4)	−0.1674(7)
0.500	−0.2864(19)	0.0308(4)	0.0640(6)	−0.1415(9)	−0.2739(12)	0.0309(3)	0.0635(5)	−0.1355(6)
0.559	−0.2114(16)	0.0229(3)	0.0477(4)	−0.1044(7)	−0.2049(11)	0.0231(2)	0.0475(3)	−0.1012(5)
0.612	−0.1630(14)	0.0176(2)	0.0367(4)	−0.0809(7)	−0.1581(10)	0.0180(2)	0.0369(3)	−0.0784(5)
0.707	−0.1064(14)	0.0113(2)	0.0241(4)	−0.0531(6)	−0.1066(10)	0.0122(2)	0.0251(3)	−0.0525(5)
0.750	−0.0877(11)	0.0096(2)	0.0199(3)	−0.0436(5)	−0.0877(8)	0.0101(1)	0.0207(2)	−0.0436(4)
0.791	−0.0745(11)	0.0083(2)	0.0175(3)	−0.0373(5)	−0.0748(8)	0.0088(1)	0.0179(2)	−0.0371(4)
0.829	−0.0625(11)	0.0071(2)	0.0148(3)	−0.0313(6)	−0.0635(8)	0.0073(1)	0.0149(2)	−0.0313(4)
0.866	−0.0522(13)	0.0060(3)	0.0123(4)	−0.0265(7)	−0.0532(9)	0.0067(3)	0.0131(3)	−0.0259(5)
0.901	−0.0456(10)	0.0053(2)	0.0107(3)	−0.0225(5)	−0.0460(6)	0.0054(2)	0.0108(2)	−0.0227(3)
0.935	−0.0389(9)	0.0044(1)	0.0092(2)	−0.0198(4)	−0.0404(6)	0.0047(1)	0.0095(2)	−0.0200(3)
1.000	−0.0303(13)	0.0036(4)	0.0068(5)	−0.0149(7)	−0.0315(11)	0.0042(3)	0.0075(4)	−0.0149(5)
1.031	−0.0266(9)	0.0032(1)	0.0066(2)	−0.0133(4)	−0.0267(5)	0.0030(1)	0.0064(2)	−0.0134(3)
1.061	−0.0222(8)	0.0026(2)	0.0054(3)	−0.0115(5)	−0.0231(6)	0.0029(1)	0.0057(2)	−0.0112(3)
1.090	−0.0192(8)	0.0022(2)	0.0048(3)	−0.0097(4)	−0.0208(7)	0.0024(1)	0.0049(2)	−0.0102(3)
1.118	−0.0183(9)	0.0022(2)	0.0043(3)	−0.0089(5)	−0.0183(8)	0.0020(2)	0.0042(3)	−0.0090(3)
1.146	−0.0159(8)	0.0017(1)	0.0036(2)	−0.0079(4)	−0.0161(6)	0.0016(1)	0.0035(1)	−0.0081(2)
1.173	−0.0137(9)	0.0016(2)	0.0033(2)	−0.0069(4)	−0.0153(6)	0.0018(1)	0.0035(2)	−0.0075(4)
1.225	−0.0118(7)	0.0017(2)	0.0030(2)	−0.0057(3)	−0.0109(6)	0.0014(1)	0.0029(2)	−0.0055(3)
1.250	−0.0090(8)	0.0012(2)	0.0021(3)	−0.0045(4)	−0.0108(7)	0.0012(1)	0.0024(2)	−0.0050(3)
1.275	−0.0079(5)	0.0012(1)	0.0021(2)	−0.0038(3)	−0.0088(5)	0.0009(1)	0.0020(1)	−0.0043(2)
1.299	−0.0079(7)	0.0009(1)	0.0018(2)	−0.0039(3)	−0.0078(6)	0.0006(1)	0.0017(1)	−0.0039(3)
1.346	−0.0067(5)	0.0009(1)	0.0018(2)	−0.0032(3)	−0.0069(5)	0.0007(1)	0.0015(1)	−0.0034(2)
1.369	−0.0054(6)	0.0006(1)	0.0013(2)	−0.0031(3)	−0.0056(6)	0.0007(1)	0.0014(2)	−0.0028(3)
1.414	−0.0035(10)	0.0003(3)	0.0008(3)	−0.0024(6)	−0.0064(7)	0.0006(2)	0.0011(2)	−0.0030(4)
1.436	−0.0035(5)	0.0004(1)	0.0007(1)	−0.0017(2)	−0.0043(5)	0.0005(1)	0.0011(1)	−0.0023(2)
1.458	−0.0038(6)	0.0003(1)	0.0008(2)	−0.0021(3)	−0.0044(5)	0.0006(1)	0.0011(1)	−0.0019(2)
1.479	−0.0030(6)	0.0005(1)	0.0008(1)	−0.0012(3)	−0.0031(6)	0.0004(1)	0.0007(1)	−0.0018(3)
1.500	−0.0015(7)	0.0001(1)	0.0005(2)	−0.0010(4)	−0.0029(6)	0.0003(1)	0.0006(2)	−0.0017(3)

TABLE XIII. Data lists of normalized free energies for all color channels at $T = 3.01T_{\rm pc}$ for $m_{\rm PS}/m_{\rm V} = 0.80$ as a function of rT.

	$T = 3.01T_{\rm pc}$, $m_{\rm PS}/m_{\rm V} = 0.80$			
rT	$V_{\mathbf{1}}$	$V_{\mathbf{8}}$	$V_{\mathbf{6}}$	$V_{\mathbf{3^*}}$
0.250	−0.8454(16)	0.0994(4)	0.2020(7)	−0.4200(9)
0.354	−0.4790(14)	0.0558(3)	0.1131(4)	−0.2376(7)
0.433	−0.3233(14)	0.0378(3)	0.0768(4)	−0.1604(6)
0.500	−0.2608(14)	0.0301(3)	0.0615(4)	−0.1295(7)
0.559	−0.1959(12)	0.0227(2)	0.0461(3)	−0.0971(6)
0.612	−0.1533(11)	0.0176(2)	0.0361(3)	−0.0761(6)
0.707	−0.1027(11)	0.0118(2)	0.0243(3)	−0.0513(5)
0.750	−0.0852(10)	0.0101(1)	0.0204(2)	−0.0424(5)
0.791	−0.0737(9)	0.0085(1)	0.0172(2)	−0.0369(5)
0.829	−0.0618(9)	0.0072(1)	0.0147(2)	−0.0306(5)
0.866	−0.0522(11)	0.0062(2)	0.0125(3)	−0.0260(5)
0.901	−0.0461(8)	0.0053(1)	0.0110(2)	−0.0230(4)
0.935	−0.0395(8)	0.0047(1)	0.0095(2)	−0.0199(4)
1.000	−0.0316(11)	0.0034(2)	0.0074(3)	−0.0160(5)
1.031	−0.0268(7)	0.0033(1)	0.0067(2)	−0.0134(3)
1.061	−0.0235(7)	0.0027(1)	0.0056(2)	−0.0118(3)
1.090	−0.0211(8)	0.0025(1)	0.0052(1)	−0.0107(4)
1.118	−0.0184(7)	0.0020(1)	0.0043(1)	−0.0094(3)
1.146	−0.0170(6)	0.0021(1)	0.0042(1)	−0.0087(3)
1.173	−0.0156(8)	0.0019(1)	0.0040(2)	−0.0081(4)
1.225	−0.0137(6)	0.0017(1)	0.0035(2)	−0.0069(3)
1.250	−0.0110(6)	0.0013(1)	0.0026(2)	−0.0056(3)
1.275	−0.0103(6)	0.0012(1)	0.0025(1)	−0.0053(3)
1.299	−0.0093(6)	0.0013(1)	0.0026(2)	−0.0049(3)
1.346	−0.0084(4)	0.0011(0)	0.0022(1)	−0.0040(2)
1.369	−0.0076(5)	0.0009(1)	0.0019(1)	−0.0039(3)
1.414	−0.0060(7)	0.0009(1)	0.0017(2)	−0.0029(3)
1.436	−0.0060(5)	0.0007(0)	0.0015(1)	−0.0031(2)
1.458	−0.0059(5)	0.0009(1)	0.0016(1)	−0.0029(2)
1.479	−0.0050(4)	0.0007(1)	0.0013(1)	−0.0023(2)
1.500	−0.0048(6)	0.0006(1)	0.0012(1)	−0.0022(3)

[1] See, e.g., K. Yagi, T. Hatsuda, and Y. Miake, *Quark-Gluon Plasma* (Cambridge University Press, Cambridge, 2005).
[2] A. Ali Khan *et al.* (CP-PACS Collaboration), Phys. Rev. D **63**, 034502 (2000).
[3] A. Ali Khan *et al.* (CP-PACS Collaboration), Phys. Rev. D **64**, 074510 (2001).
[4] Y. Iwasaki, K. Kanaya, S. Kaya, and T. Yoshie, Phys. Rev. Lett. **78**, 179 (1997).
[5] R. D. Pisarski and F. Wilczek, Phys. Rev. D **29**, 338 (1984).
[6] K. Rajagopal and F. Wilczek, Nucl. Phys. **B399**, 395 (1993).
[7] A. Ali Khan *et al.* (CP-PACS Collaboration), Phys. Rev. Lett. **85**, 4674 (2000).
[8] A. Ali Khan *et al.* (CP-PACS Collaboration), Phys. Rev. D **65**, 054505 (2002).
[9] O. Kaczmarek, F. Karsch, E. Laermann, and M. Lutgemeier, Phys. Rev. D **62**, 034021 (2000).
[10] A. Nakamura and T. Saito, Prog. Theor. Phys. **111**, 733 (2004).
[11] A. Nakamura and T. Saito, Prog. Theor. Phys. **112**, 183 (2004).
[12] O. Kaczmarek and F. Zantow, Phys. Rev. D **71**, 114510 (2005).
[13] M. Döring, S. Ejiri, O. Kaczmarek, F. Karsch, and E. Laermann, Eur. Phys. J. C **46**, 179 (2006).
[14] V. G. Bornyakov *et al.* (DIK Collaboration), Phys. Rev. D **71**, 114504 (2005).
[15] M. Laine, O. Philipsen, P. Romatschke, and M. Tassler, hep-ph/0611300.
[16] T. Matsui and H. Satz, Phys. Lett. B **178**, 416 (1986).
[17] G. S. Bali, J. Fingberg, U. M. Heller, F. Karsch, and K. Schilling, Phys. Rev. Lett. **71**, 3059 (1993).

[18] L. Kärkkäinen, P. Lacock, D. E. Miller, B. Petersson, and T. Reisz, Phys. Lett. B **312**, 173 (1993).
[19] F. Karsch, E. Laermann, and M. Lutgemeier, Phys. Lett. B **346**, 94 (1995).
[20] G. Boyd, J. Engels, F. Karsch, E. Laermann, C. Legeland, M. Lutgemeier, and B. Petersson, Nucl. Phys. **B469**, 419 (1996).
[21] M. Laine and Y. Schröder, J. High Energy Phys. 03 (2005) 067.
[22] Y. Iwasaki, Nucl. Phys. **B258**, 141 (1985); University of Tsukuba Report No. UTHEP-118, 1983 (unpublished).
[23] B. Sheikholeslami and R. Wohlert, Nucl. Phys. **B259**, 572 (1985).
[24] S. Aoki, Phys. Rev. D **30**, 2653 (1984).
[25] S. Aoki, Phys. Rev. Lett. **57**, 3136 (1986).
[26] S. Aoki, Nucl. Phys. **B314**, 79 (1989).
[27] S. Aoki, A. Ukawa, and T. Umemura, Phys. Rev. Lett. **76**, 873 (1996).
[28] S. Aoki, T. Kaneda, A. Ukawa, and T. Umemura, Nucl. Phys. B, Proc. Suppl. **53**, 438 (1997).
[29] S. Nadkarni, Phys. Rev. D **33**, 3738 (1986).
[30] S. Nadkarni, Phys. Rev. D **34**, 3904 (1986).
[31] S. Aoki *et al.* (CP-PACS Collaboration), Phys. Rev. D **60**, 114508 (1999).
[32] M. Göckeler *et al.*, Phys. Rev. D **73**, 014513 (2006).
[33] A. Nakamura, T. Saito, and S. Sakai, Phys. Rev. D **69**, 014506 (2004).
[34] A. K. Rebhan, Phys. Rev. D **48**, R3967 (1993).
[35] G. P. Lepage and P. B. Mackenzie, Phys. Rev. D **48**, 2250 (1993).
[36] O. Jahn and O. Philipsen, Phys. Rev. D **70**, 074504 (2004).
[37] T. Umeda, Proc. Sci., LAT2006 (2006) 151.
[38] Y. Schröder and M. Laine, Proc. Sci., LAT2005 (2006) 180.
[39] S. Ejiri *et al.*, Proc. Sci., LAT2006 (2006) 132.
[40] Y. Maezawa *et al.*, hep-lat/0702005